OULUN YLIOPISTO
UNIVERSITY of OULU

DEPARTMENT OF COMPUTER SCIENCE AND ENGINEERING

Juha Okkonen

UNIFORM LINEAR ADAPTIVE ANTENNA ARRAY BEAMFORMING IMPLEMENTATION WITH A WIRELESS OPEN-ACCESS RESEARCH PLATFORM

Master's Thesis
Degree Programme in Computer Science and Engineering
May 2013

Okkonen J. (2013) Uniform linear adaptive antenna array beamforming implementation with a wireless open-access research platform. University of Oulu, Department of Computer Science and Engineering. Master's Thesis, 58 p.

ABSTRACT

The wireless communication techniques are expected to keep up with the increasing demand for capacity. The increased number of users is the primary culprit with the contribution of more data intensive applications. Multiple access divisions based on time, frequency and code have been widely explored and space remains the most promising option for future capacity improvements.

Beamforming is an advanced space division multiple access (SDMA) technique, where an array of antennas spatially filters signals based on their capture time at each element. Unless the signal arrives orthogonally at the array, the capture times differ based on the direction of arrival (DOA).

Two non-adaptive beamforming techniques were implemented with a wireless open-access research platform (WARP). The first technique was the conventional beamforming, where the main beam is steered towards the DOA. The second technique was the null-steering beamforming, where, in addition to steering the main beam, minimum gains (nulls) are placed towards interfering sources for suppression.

The measured beamforms, for receive beamforming, yielded a good main beam performance with respect to the theoretical beamforms, although the null-steering had some deviations. The null levels were about -20 dB and -28 dB for the conventional and null-steering beamforming, respectively. Sidelobe levels were slightly higher, at around -10 dB, and wider for the conventional beamforming. In the null-steering, the sidelobe levels were somewhat or considerably higher and wider depending on the placement of nulls.

Keywords: adaptive antenna, beamforming, phased array, SDMA, smart antenna, uniform linear array, wireless open-access research platform

Okkonen J. (2013) Tasavälisen lineaarisen adaptiivisen antenniryhmän keilanmuodostuksen toteutus langattomalla tutkimusalustalla. Oulun yliopisto, Tietotekniikan osasto. Diplomityö, 58 s.

TIIVISTELMÄ

Langattomilta tietoliikennetekniikoilta oletetaan yhä suurempaa kapasiteettia. Lisääntyneet käyttäjämäärät ovat suurin tekijä, mutta osansa on myös sovelluksien suuremmilla tiedonsiirtovaatimuksilla. Aika-, taajuus- ja koodijakokanavoinnit ovat laajasti tutkittuja ja tilajakokanavointi (SDMA, space division multiple access) on lupaavin vaihtoehto kapasiteetin kasvattamiselle tulevaisuudessa.

Keilanmuodostus on kehittynyt tilajakokanavointitekniikka, jossa antenniryhmä erottelee signaalit avaruudessa eri antennien vastaanottoaikojen perusteella. Ellei signaali saavu ortogonaalisesti antenniryhmälle, vastaanottoajat eroavat toisistaan riippuen signaalin tulosuunnasta (DOA, direction of arrival).

Kaksi ei-adaptiivista keilanmuodostustekniikkaa toteutettiin langattomalla tutkimusalustalla (WARP, wireless open-access research platform). Ensimmäinen tekniikka oli klassinen keilanmuodostus, jossa pääkeila suunnataan kohti signaalin tulosuuntaa. Toinen tekniikka oli nollanohjausmenetelmä, jossa, pääkeilan suuntaamisen lisäksi, minimivahvistukset (nollat) suunnataan kohti häiriölähteitä niiden vaimentamiseksi.

Vastaanotossa mitatut keilanmuodot saavuttivat hyvän suorituskyvyn verrattaessa niitä teoreettisiin keilanmuotoihin. Nollanmuodostusmenetelmällä oli kuitenkin pieniä poikkeavuuksia. Nollatasot olivat noin -20 dB klassisella keilanmuodostuksella ja -28 dB nollanohjausmenetelmällä. Sivukeilatasot olivat hieman korkeammat, -10 dB tasolla, ja leveämmät klassisessa keilanmuodostuksessa. Nollanohjausmenetelmässä sivukeilatasot olivat hieman tai merkittävästi korkeammat ja leveämmät riippuen nollien sijoitteluista.

Avainsanat: adaptiivinen antenni, keilanmuodostus, langaton tutkimusalusta, tasavälinen lineaarinen ryhmä, tilajakokanavointi, vaiheistettu antenniryhmä, älyantenni

TABLE OF CONTENTS

FOREWORD

The research work for this master's thesis was carried out at the Centre for Wireless Communications (CWC), Department of Communications Engineering (DCE), University of Oulu. The thesis is part of a Reconfigurable Antenna Based Enhancement of Dynamic Spectrum Access Algorithms (RADSA) research project that was conducted in co-operation with the CWC and the Drexel University in Philadelphia, Pennsylvania, USA. The purpose of this thesis was to develop a reconfigurable direction selective antenna system, capable of directed transmission and reception, through adaptive antenna beamforming that was demonstrated with the Wireless Open-Access Research Platform (WARP) environment.

I would like to express thanks to my supervisors M.Sc. Hannu Tuomivaara for his guidance and advice and Dr. Harri Saarnisaari for his insight and feedback. I am very grateful to Lic.Sc. Pekka Lilja, M.Sc. Marko Sonkki and Lic.Sc. Risto Vuohtoniemi for their assistance.

I would like to thank my fellow team members for a comfortable working atmosphere, especially M.Sc. Markku Jokinen for his help with the equipment. My thanks go to the second examiner Dr. Timo Ojala for his comments and Dr. Pekka Pirinen for giving the opportunity to work at the CWC.

I also thank M.Sc. Jari Sillanpää for technical support, M.Sc. Tuomo Hänninen for supervision and the whole staff at the DCE including administrative personnel.

The research funding provided by the Finnish Funding Agency for Technology and Innovation (TEKES) is gratefully acknowledged.

Special thanks to my family and friends for their support.

Oulu, May 22th, 2013

Juha Okkonen

LIST OF SYMBOLS AND ABBREVIATIONS

$[\cdot]^+$	matrix pseudo inverse
$[\cdot]^*$	complex conjugate
$[\cdot]^{-1}$	matrix inversion
$[\cdot]^H$	complex conjugate transpose
$[\cdot]^T$	transpose
π	mathematical constant, ratio of a circle's circumference to its diameter
$\in$	set membership operator
$e^{[\cdot]}$	exponential function
$\sum$	summation operator
$\lvert \cdot \rvert$	absolute value
$E\{\cdot\}$	expectation operator
$\log_{10}$	common logarithm
$\max[\cdot]$	maximum value
$\mathbf{a}(\theta)$	steering vector as a function of incident angle
$\mathbf{a}(\omega)$	steering vector as a function of angular frequency
$\mathbf{A}$	steering matrix
c	speed of light
d	element spacing
f	frequency
$\mathbf{I}$	identity matrix
k	wave number
M	number of signal sources
$n_m(t)$	noise at mth element
N	number of elements in an array
p_i	ith signal source power measured at one the elements of the array
p_s	signal source power
$P(\theta)$	beamformer response as a function of incident angle
$P(\omega)$	beamformer response as a function of angular frequency
$\mathbf{P}(\mathbf{w})$	beamformer mean output power
$\mathbf{P}_N$	beamformer output noise power
r	radial distance from origin
$\mathbf{R}$	correlation matrix
$\mathbf{R}_N$	noise correlation matrix
$s_i(t)$	ith signal
SNR_{in}	beamformer input signal-to-noise ratio
SNR_{out}	beamformer output signal-to-noise ratio
$\mathbf{S}$	source correlation matrix
t	time
w_m^*	complex weight for mth antenna element
$\mathbf{w}$	weight vector
$\mathbf{w}_C$	weight vector for conventional beamformer
$\mathbf{w}_{NS}$	weight vector for null-steering
x	first coordinate in Cartesian system

$x_m(t)$	output of m antenna element
$x_{ms}(t)$	signal induced on the mth element due to signal source s
X	number of phase offset measurement
$\mathbf{x}(t)$	all the signals induced on all the elements
$\mathbf{x}_s(t)$	signal induced on all the elements in the array due to signal source s
y	second coordinate in Cartesian system
$y(t)$	beamformer output
z	third coordinate in Cartesian system
α_i	PLL phase offset of radio board i
δ	PLL phase offset change due to propagation of signal in channel
θ	zenith angle
θ_i	angle of incidence
θ_{rfl}	angle of reflection
θ_{rfr}	angle of refraction
λ	wavelength
σ_n^2	noise variance
τ_m	propagation delay to mth antenna with respect to first
ϕ	azimuth angle
ω	angular frequency
AAS	active antenna system
ADC	analog-to-digital converter
AF	array factor
AGC	automatic gain control
CF	CompactFlash
CWC	Centre for Wireless Communications
DAC	digital-to-analog converter
dB	decibel
DBF	digital beamforming/beamformer
DCE	Department of Communications Engineering
DIP	dual in-line package
DOA	direction of arrival
EM	electromagnetic
FPGA	field-programmable gate array
Gbps	gigabits per second
GHz	gigaHertz
I	in-phase
I/O	input/output
I/Q	in-phase/quadrature
IF	intermediate frequency
ISM	industrial, scientific and medical
JTAG	Joint Test Action Group
kb	kilobit
LED	light-emitting diode
LOS	line-of-sight
M2M	machine-to-machine

MAC	medium access control
MATLAB	matrix laboratory
Mb	megabit
Mbps	megabits per second
MGT	multi-gigabit transceiver
MHz	megaHertz
MIMO	multiple input multiple output
MMSE	minimum mean square error
MRA	minimum redundancy array
NLOS	non-line-of-sight
NNBW	null-to-null beamwidth
NRA	null redundancy array
NSN	Nokia Siemens Networks
OTA	over-the-air
PC	personal computer
PHY	physical layer
PLL	phase-locked loop
Q	quadrature-phase
RADSA	Reconfigurable Antenna Based Enhancement of Dynamic Spectrum Access
RAM	random access memory
RF	radio frequency
RP	radiation pattern
RS-232	recommended standard 232
RSSI	received signal strength indicator
Rx	receiver / reception / receive
SDMA	space-division multiple access
SIR	signal-to-interference ratio
SNR	signal-to-noise ratio
SPI	Serial Peripheral Interface
SRAM	static random access memory
TEKES	Finnish Funding Agency for Technology and Innovation
Tx	transmitter / transmission / transmit
UART	Universal Asynchronous Receiver Transmitter
UCA	uniform circular array
ULA	uniform linear array
USB	Universal Serial Bus
V	volt
WARP	Wireless Open-Access Research Platform
ZBT	zero-bus-turnaround

1. INTRODUCTION

The wireless communications is facing an enormous challenge to satisfy the ever-increasing demand for capacity. The demand is primarily caused by an increasing number of users but also because of more data intensive applications. It is expected that the number of mobile Internet-connected devices is over 10 billion in 2016, exceeding the number of people on Earth, estimated to be 7.3 billion. 8 billion of these are personal mobile-ready devices and the remaining 2 billion are machine-to-machine (M2M) connections. The devices will be more powerful and hence are able to consume and generate more data traffic. From 2011 to 2016, the mobile data traffic will increase 18-fold, streamed content 28-fold and tablet traffic 62-fold. Smartphones, laptops and other portable devices will be responsible for about 90 % of all mobile data traffic by 2016. Remaining 10 % belongs to M2M communication and residential broadband mobile gateways, 5 % each. Mobile video alone, is 71 % of all mobile data traffic. Mobile data traffic is expected to outgrow fixed data traffic by three times by the end of 2016. [1]

Interference is one of the major problems in radio communications. The interference can be caused by the signal itself or by other users [2]. Signal can interfere with itself due to multipath components, where the signal is combined with another version of the signal that is delayed because of another propagation path. Interference from other users can be either unintentional or intentional [2]. Unintentional interference is caused by nonidealities in the transmitter or using the same or adjacent channel. Intentional interference or jamming is radiation directed towards a target for the purpose of trying to prevent it from receiving the desired signal.

Transmitted signals can be separated from each other in time, frequency, code and space. Divisions based on time, frequency and code have been widely studied and only space-division multiple access (SDMA) remains to be exploited for future capacity improvements [3]. In SDMA, spectrally and temporally overlapping signals from different origin can be filtered in the spatial domain (Figure 1) [4]. SDMA can be further subdivided into different methods: sectorization, switched beam systems, fixed multiple beam systems, adaptive arrays and multiple input multiple output (MIMO) techniques.

An adaptive array is also known as a smart antenna. In this thesis, an adaptive array refers to an array of antennas, which are controlled adaptively. A smart antenna, although being a synonym for adaptive array, will refer to a wider set of antennas, that adaptive array is a part of.

Sectorization has been the most commonly used spatial technique in mobile communication systems for years in an attempt to reduce interference and increase capacity. Cells are divided into three or six sectors, for example. Each sector is equipped with a dedicated antenna and radio frequency (RF) path. By increasing the amount of sectorization, interference that is seen by the desired signal can be reduced. At the same time, efficiency decreases because antenna patterns overlap more. Another drawback is the increased number of handoffs for mobile users travelling within a cell as the sector count is increased. [5]

Early smart antenna types include the switched beam (Figure 2 a)) and multiple fixed beam systems (Figure 2 b)). The switched beam method extends the sectorization. Macro-sectors are further divided into several micro sectors. Each micro sector has

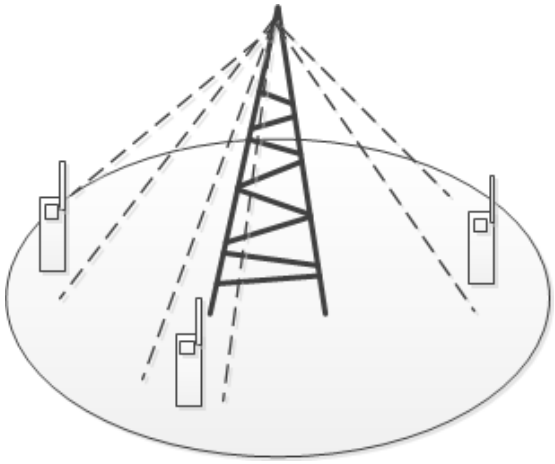

Figure 1. Spatial division multiple access.

a predetermined fixed beam pattern, where the greatest gain is directed towards the center of the beam. The system selects a beam with the strongest signal and switches to other beams as needed. The switched beam system has a low complexity, cost and base stations require only a little modification. Coverage is extended due to a gain from the antenna array aperture. The switched beam system is vulnerable to interfering signals or multipath components arriving from almost the same angle as the desired signal. These signals appear in the same output port with the desired signal and they are difficult to separate. The switched beam system is affected by a phenomenon known as scalloping, where the antenna array gain drops as a function of the direction of arrival (DOA) as the angle moves away from the beam center towards the intersection of two beams. This causes mobile user's signal to change accordingly as it moves between the coverage of beams. The switched beam system does not utilize path diversity. Only one signal is selected based on its strength and the rest are omitted. The multiple fixed beam system extends previous by combining signals from all ports, hence utilizing path diversity. [5]

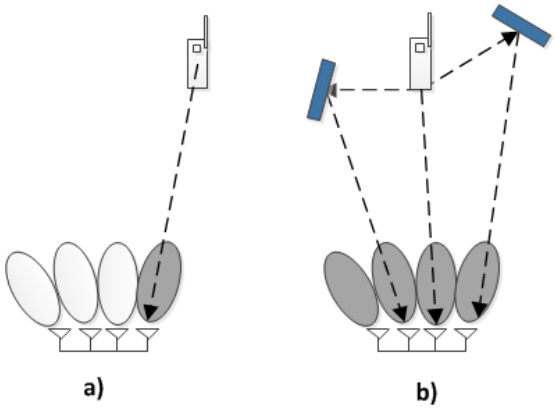

Figure 2. Basic smart antenna techniques. (a) Switched beam system. (b) Multiple fixed beam system.

While previous methods utilized multiple beams and changed between them as needed, in adaptive arrays (Figure 3 a)) a beam can be steered towards desired users and nulls placed towards interfering signals. Finally, adaptive arrays can be used in both transmission (Tx) and reception (Rx) side, giving rise to the MIMO systems (Figure 3 b)). The latter mentioned methods offer greater performance but at the cost of increasing complexity. [5]

One of the latest promising improvements is an active antenna system (AAS), that has been pioneered by Nokia Siemens Networks (NSN). The NSN has demonstrated working AAS examples since the technology was first introduced in 2008. In AAS the performance is increased by integrating base station's RF elements into the antenna. Through beamforming, the AAS aims to meet the dynamic demands of mobile customers more cost-effectively than using conventional passive antennas. [6]

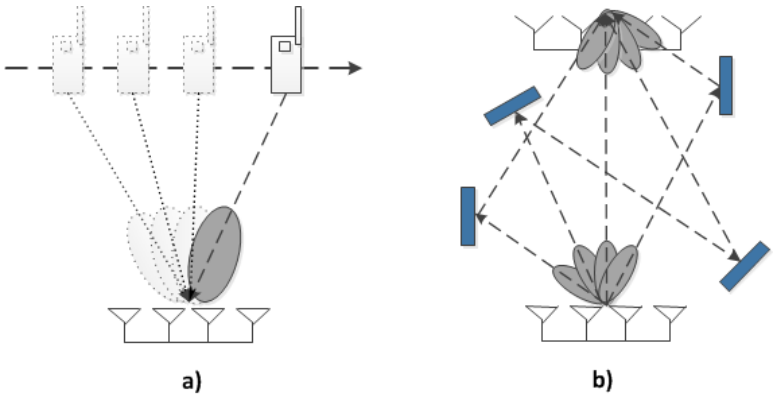

Figure 3. Advanced smart antenna techniques. (a) Adaptive array. (b) MIMO.

Beamforming is a process where an array of antennas is utilized together to spatially filter incident wavefront in order to enhance its amplitude relative to the background noise and directional interference [7]. The array is formed by a combination of small non-directional, or directional, antennas [8]. For each element, the signal arrival time depends on the DOA and the spacing between elements. Unless the DOA is orthogonal to the linear array, the signal arrival times differ. When the signals from all the elements are summed together coherently, the array has a diversity gain. This array of antennas, known as a smart or adaptive antenna, can be regarded as an ultimate antenna that captures all the information while separating information of interest via signal processing [3].

Adaptive antennas offer numerous benefits. These can be divided into improvements relating to diversity gain and directionality. The gain improves the signal-to-interference ratio (SIR), which leads to many improvements. A higher capacity and peak data rates can be supported because more complex modulation can be used. The range increases and the base station has better coverage. Less power can be used for transmission. The costs are reduced as a result of longer battery life and extended coverage. A building penetration is better and immunity to near-far problems increases. Adaptive antennas have directionality, which helps with the interference management. On reception, less interference is seen because the signals from a specific direction are received with a higher gain than from other directions. On the other hand, on transmission, less interference is caused to the environment because the electromagnetic

energy is more focused. The array can take advantage of spatial, polarization and angular diversity to minimize the effects of a multipath propagation, e.g., fading. Arrays can be electronically steered, which is a major advantage over mechanically steered antennas. Mechanically steered antennas have a large inertia and it may take seconds to reposition the antenna whereas with electronic circuits the steering can be done in microseconds or less. Steering can be used to position the antenna for optimal transmit or receive conditions. In addition, the number of beams is not limited to one as is with the conventional antennas. Therefore, a separate beam can be generated for each user that minimizes the noise to or from others. [4, 5, 9–12]

Beamforming has been used for decades in radar and sonar, where it has spread in new applications. Early beamforming uses were air traffic control (radar), and source localization and classification (sonar). Figure 4 [3, 5, 9, 13–15] illustrates different applications where beamforming has been used. [3, 15]

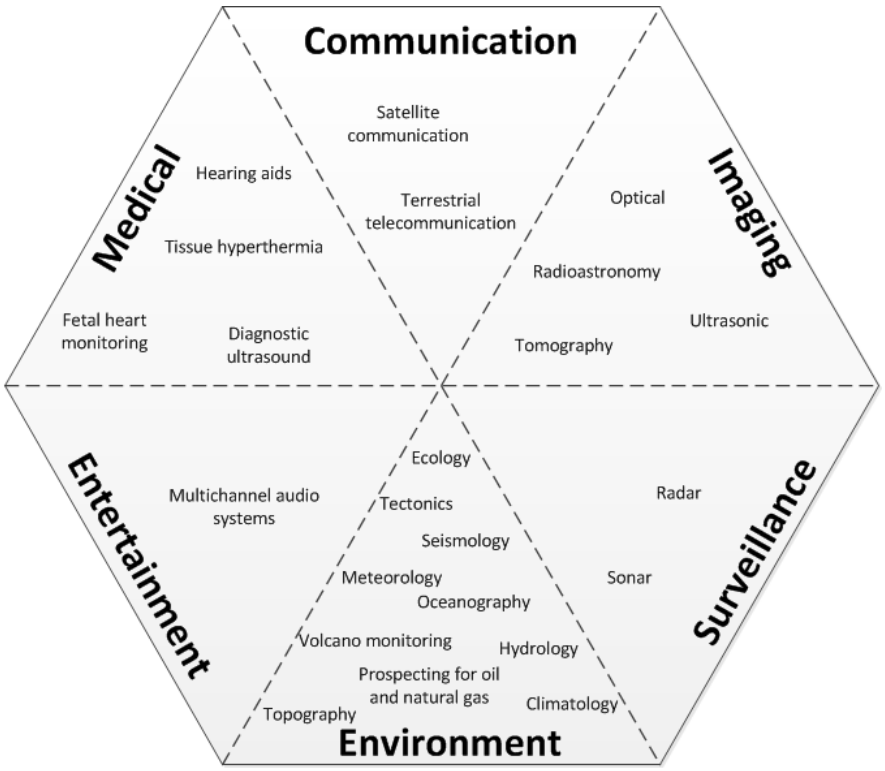

Figure 4. Applications of beamforming.

This thesis is a part of the RADSA research project that is carried out in co-operation with the CWC and Drexel University. It aims to major performance improvements in cognitive radio networks by utilizing directed transmissions. The main tasks of the project include the development of a reconfigurable direction selective antenna system, cognition based on a dynamic spectrum access and directed transmission and reception, and demonstration of the former with the WARP environment. The focus of this thesis is the development of a reconfigurable antenna system capable of directed transmission and reception through adaptive antenna beamforming. The realization was with a four-element antenna array connected to a WARP board that is controlled with the MATrix LABoratory (MATLAB [16]), a high-level language and environment for

numerical computation, visualization and programming. The implementation utilized the channel 14 (2484 MHz) of the 2.4 GHz industrial, scientific and medical (ISM) band.

The outline of this thesis is as follows. Chapter 2 illustrates the beamforming concept in detail and the beamforming methods used in the implementation. In Chapter 3, the WARP board is introduced. Description of the calibration can be found in Chapter 4. Measurements are presented in Chapter 5. Finally, a discussion and summary are given in Chapters 6 and 7, respectively.

2. BEAMFORMING

Beamforming, along with many other technologies, has evolved from an analog to a digital format. Performing beamforming in a digital domain rather than analogically at RF or intermediate frequency (IF) introduces many benefits. Digital beamforming (DBF) allows the control of the antenna array's radiation pattern accurately at high clock frequencies. The beam's direction and shape can be changed fast. Rapid reconfigurability enables the implementation of adaptive algorithms, beam scanning and self-calibration. Generation of multiple simultaneous beams, that may overlap, is possible with DBF. Multiple beams can be used, for example, in multipath discrimination. In analog beamforming, the propagation time differences between array elements are compensated with time delays whereas in DBF it can be accomplished by controlling the amplitudes and phases. [4, 9, 13, 17]

A conventional beamformer uses a single parabolic dish antenna (Figure 5 a)) and is capable of producing a single beam. It amplifies signals from the direction it is pointed at and attenuates those from other directions. For high spatial discrimination, the aperture needs to be large in terms of wavelength. Mechanical operation for direction selection limits the number of trackable signals to one and the change of direction is slow due to a physical repositioning of the dish. Furthermore, the response is fixed. These restraints and the increase in requirements have lead to the development of adaptive arrays, also known as phased arrays (Figure 5 b)). In a phased array, the direction of focus is controlled by weighting the outputs of the array antennas. With DBF, the direction is easily changed fast and multiple beams can be generated. The phased array can remain stationary as the listening direction is almost independent of the orientation of the array. A phased array's response can be adaptively changed, e.g., to combat emerging strong interference. Phased arrays are preferred over the conventional dish antennas because they require less space. A phased array's maximum azimuth coverage is usually $\pm 60^{\circ}$ and multiple arrays can be combined to fulfill the coverage requirements. However, phased arrays are not without their downsides. The shape of the resulting beam varies as a function of the direction which it is pointing at. Its bandwidth is narrower than a conventional beamformer's. Also, the design and manufacturing are more expensive. [13, 14, 18]

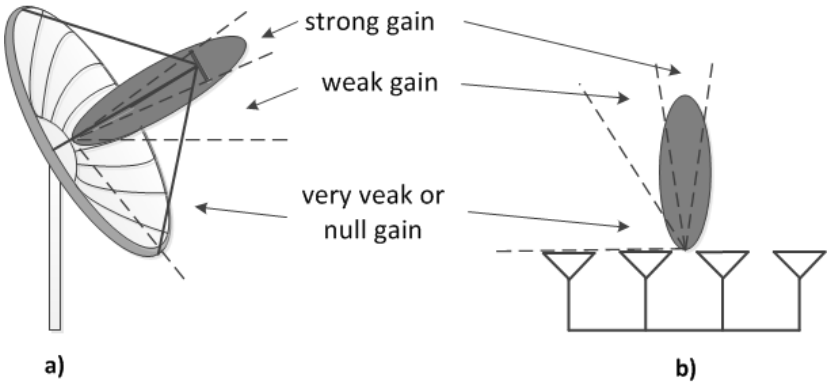

Figure 5. Antennas for beamforming. (a) Parabolic dish antenna. (b) Phased array.

A single antenna can separate signals using time, frequency or code information. If two or more signals share the same attributes, for example they are using the same frequency, and arrive at the antenna at the same time, the antenna is unable to decide them apart. If the receiver uses more than one antenna, it can take advantage of spatial information. For the same scenario as before, incoming signals may share the same attributes but if they arrive from different directions, they can be differentiated because they arrive at different antennas at different times. An adaptive antenna is formed by combining the information from multiple antennas together. This combination of antennas is called an array and it can take many shapes.

This Chapter provides understanding about the beamforming. In Section 2.1, a coordinate system is defined that forms the basis for beamforming. Section 2.2 introduces the principle of beamforming. Issues relating implementation are discussed in Section 2.3. The performance of beamformer is affected by several factors and these are considered in Section 2.4. Finally, beamforming techniques used in this thesis are introduced in Section 2.5.

2.1. Coordinate system

The most commonly known coordinate system is a Cartesian system, which specifies the location in space with three coordinates, i.e., (x, y, z). In the context of antennas, it is not intuitive and a better alternative is to use a spherical coordinate system. The spherical coordinates are also specified with three variables, i.e., (r, ϕ, θ), where r is the radial distance, or range, from origin, ϕ is the azimuth angle and θ is the elevation, or more commonly known as a polar or zenith angle. Figure 6 relates these coordinate systems.

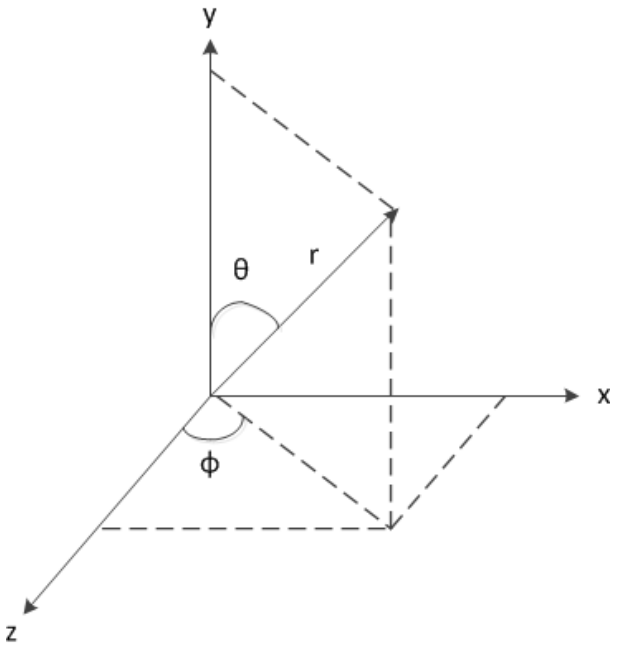

Figure 6. Relation between the Cartesian and the spherical coordinate system.

2.2. Operating principle

Electromagnetic (EM) signals are generated by the moving charged particles. As the name suggests, it consists of two parts: an electric and magnetic component. These components oscillate perpendicular to each other and in the direction of propagation. A signal propagates as an EM wave through medium such as air, water or vacuum. In a vacuum, wave travels with the speed of light. EM radiation induces a voltage to the receiving antenna. A transmitting antenna operates in reverse by causing an EM radiation as a result of applied voltage.

2.2.1. Fundamentals

Beamforming is based on the wave behavior of EM waves. The waves interact with each other through interference that may be either constructive or destructive. In beamforming, the waves are combined constructively on some angles while for other angles they combine destructively [19]. Figure 7 depicts the principle of beamforming for a uniform linear array (ULA).

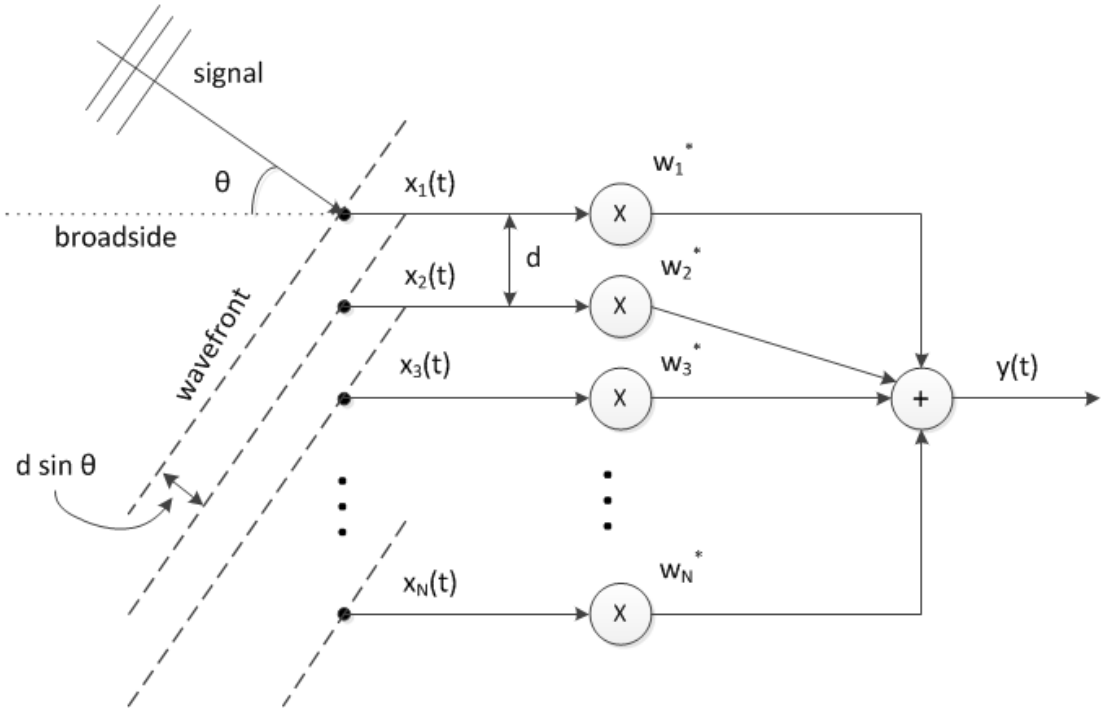

Figure 7. Beamforming principle with a uniform linear array.

The signal impinges on the array from an angle θ relative to the broadside, which is the direction perpendicular to the array. The signal is an EM wave that arrives as a wavefront, assuming the array is in the far-field of the radiating source. The array has N elements and they are spaced distance d apart. Each of the elements sample the incident EM wave, that is a spatiotemporal signal, and convert it to a temporal signal [20]. Because the DOA of the signal is different from that of the broadside, the

signal arrives at different times to the different antenna elements. The signal reaches first the topmost element with index 1. The distance the wave has to travel to the next element is a function of the element spacing d and incident angle θ and is equal to $d \sin \theta$.

By weighting the signals from each antenna, it is possible to focus on signals arriving from a particular direction [14]. Beamforming weights are discussed in more detail in Section 2.5. The output of the beamformer is given by

$$y(t) = \sum_{m=1}^{N} w_m^* x_m(t), \tag{1}$$

where $y(t)$ is the output of the beamformer, $x_m(t)$ is the output of the antenna element m, w_m^* is the complex weight for the antenna element m, $m = 1, 2, \ldots, N$ and $[\cdot]^*$ denotes the complex conjugate.

2.2.2. Radio channel propagation

The propagation of a radio signal from a transmitter to a receiver may not have a line-of-sight (LOS) when the radio channel is obstructed with, e.g., buildings, mountains, hills, trees, foliage or moving objects [5, 21]. The obstructions are responsible for the propagation phenomena like reflection, refraction, diffraction and scattering [21]. Figure 8 illustrates these phenomena. In reflection (Figure 8 a)) the incident EM wave changes its direction upon encountering an object with large dimensions, compared to the wavelength of the EM wave. The new direction is such that the angle of reflection, θ_{rfl}, is mirrored from the angle of incidence, θ_i, with respect to the normal. Refraction (Figure 8 b)) is a change in direction because of an EM wave entering a different medium. The angle of refraction, θ_{rfr}, will be closer to the normal or further away from the normal than the angle of incidence, θ_i, depending on how dense the entered medium is compared to the left medium. Upon encountering sharp edges of a surface, the EM wave experiences a diffraction (Figure 8 c)). The EM wave will not only continue on its original path, with LOS, but it will also propagate towards the non-line-of-sight (NLOS) side of the surface. Scattering (Figure 8 d)) is caused by irregularities in the radio channel, e.g., rough surfaces. The incident wave bounces off the surface and multiple waves continue in slightly different directions.

As a result of propagation phenomena in a radio channel, the radio waves arrive at the receiver from different directions with different amplitude, phase and time delay. The combined effect, of all the phenomena, is referred to as a multipath propagation. [21]

2.2.3. Signal model

In this section, the ULA beamformer, shown in Figure 7, is analyzed and the signal model adopted is presented. The beamformer consists of N omnidirectional antenna

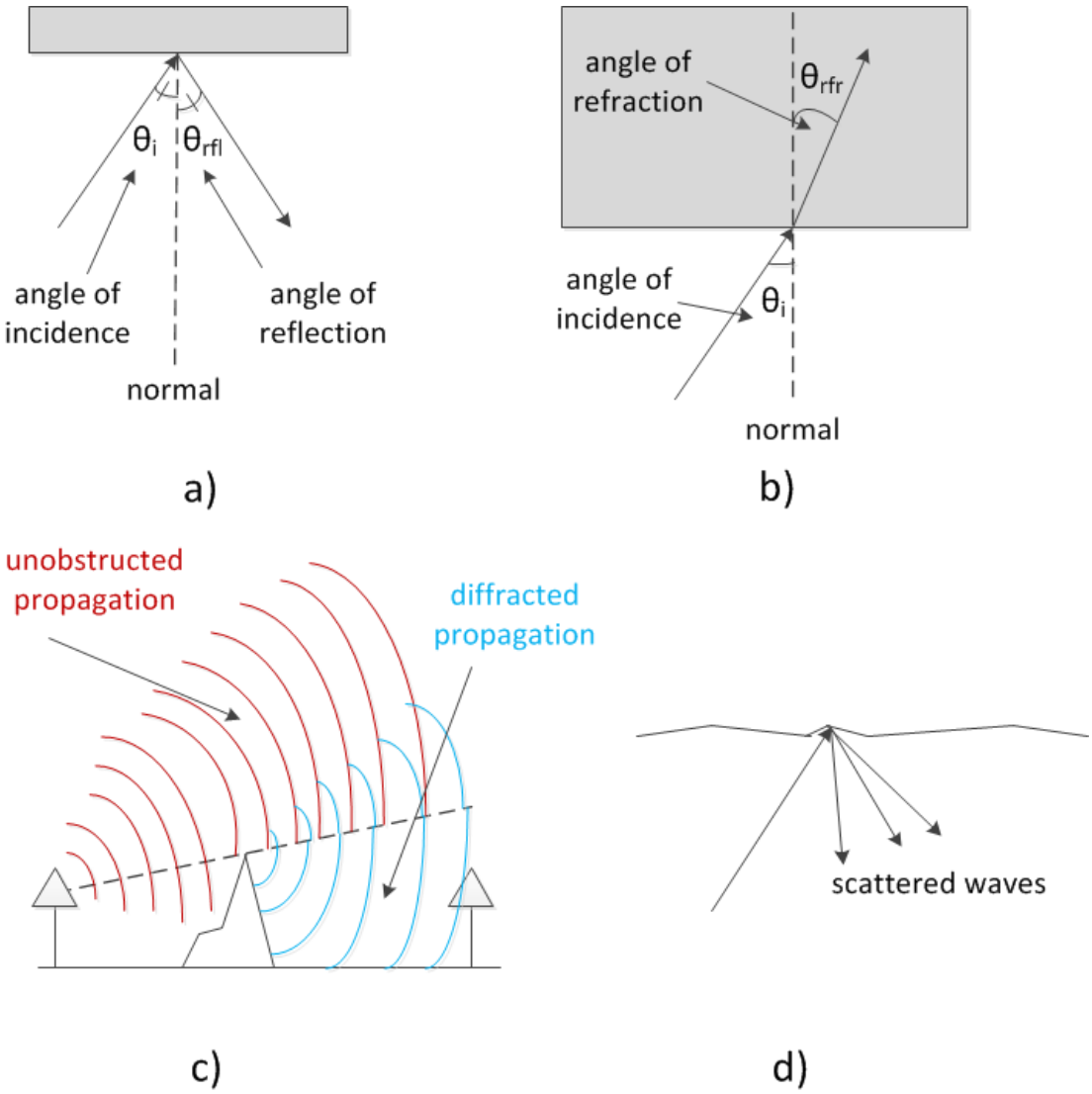

Figure 8. Radio propagation phenomena. (a) Reflection. (b) Refraction. (c) Diffraction. (d) Scattering.

elements spaced distance d apart. The propagation delay $\tau_m(\theta)$ for an impinging signal from the first antenna to the mth, with DOA of θ, is

$$\tau_m(\theta) = \frac{(m-1)d\sin\theta}{c}, \tag{2}$$

where θ is the incident angle, $\theta \in [-\pi/2 \quad \pi/2]$ and c is the speed of light [22].

The impinging signal is assumed to be a complex plane wave of the form

$$s_i(t)e^{j\omega t}, \tag{3}$$

where $s_i(t)$ is the ith signal and ω is the angular frequency.

The wavefront arrives at the mth element $\tau_m(\theta)$ seconds later than at the first element. Hence the signal induced on the mth element due to the ith source is expressed as

$$s_i(t)e^{j\omega(t-\tau_m(\theta_i))}. \tag{4}$$

The total signal, $x_m(t)$, induced due to all M sources and noise on the mth element, is given by

$$x_m(t) = \sum_{i=1}^{M} s_i(t) e^{j\omega(t-\tau_m(\theta_i))} + n_m(t), \tag{5}$$

where $n_m(t)$ is the noise at the mth element. The noise is assumed to be white Gaussian noise with variance equal to σ_n^2. The noise at different antenna elements is independent. [23]

The output of the beamformer given in (1) can be written in vector format as

$$y(t) = \mathbf{w}^H \mathbf{x}(t), \tag{6}$$

where $[\cdot]^H$ denotes the Hermitian (complex conjugate) transpose, $\mathbf{w}$ is the weight vector, with N complex coefficients, of the array given as

$$\mathbf{w} = [w_1 \quad w_2 \quad \dots \quad w_N]^T, \tag{7}$$

where $[\cdot]^T$ denotes the transpose and $\mathbf{x}$ is the vector of signals induced on all the elements as

$$\mathbf{x}(t) = [x_1(t) \quad x_2(t) \quad \dots \quad x_N(t)]^T. \tag{8}$$

Throughout this thesis, vectors and matrices are denoted with boldface lowercase and uppercase letters, respectively. [22, 23]

Assuming the elements of $\mathbf{x}(t)$ are zero mean stationary processes, the mean output power of the beamformer is

$$P(\mathbf{w}) = E\{y(t)y^H(t)\} = \mathbf{w}^H \mathbf{R} \mathbf{w}, \tag{9}$$

where $E\{\cdot\}$ denotes the expectation operator and $\mathbf{R}$ is the array correlation matrix defined as

$$\mathbf{R} = E\{\mathbf{x}(t)\mathbf{x}^H(t)\}. \tag{10}$$

Through algebraic manipulation of (5), (8) and (10), the correlation matrix, $\mathbf{R}$, can be written as

$$\mathbf{R} = \sum_{i=0}^{M-1} p_i \mathbf{a}_i(\omega)\mathbf{a}_i^H(\omega) + \sigma_n^2 \mathbf{I}, \tag{11}$$

where p_i denotes the power of the ith source measured at one of the elements of the array, $\mathbf{a}_i(\omega)$ is the steering vector for ith source and $\mathbf{I}$ denotes an identity matrix. The correlation matrix can be expressed in a matrix notation as

$$\mathbf{R} = \mathbf{A}\mathbf{S}\mathbf{A}^H + \sigma_n^2 \mathbf{I}, \tag{12}$$

where matrix $\mathbf{A}$ consists of steering vectors as

$$\mathbf{A} = [\mathbf{a}_0(\omega) \quad \mathbf{a}_1(\omega) \quad \dots \quad \mathbf{a}_{M-1}(\omega)] \tag{13}$$

and $\mathbf{S}$ is the source correlation matrix. [23]

The steering vector $\mathbf{a}_i(\omega)$ is given by

$$\mathbf{a}_i(\omega) = [1 \quad e^{-j\omega\tau_2(\theta)} \quad \dots \quad e^{-j\omega\tau_N(\theta)}]^T. \tag{14}$$

The steering vector $\mathbf{a}_i(\omega)$ can also be expressed in another form by substituting ω with $2\pi f$ and (2) into (14). This yields

$$\omega\tau_m(\theta) = 2\pi f\frac{(m-1)d\sin\theta}{c} = k(m-1)d\sin\theta, \tag{15}$$

where k is the wave number, given as

$$k = \frac{2\pi}{\lambda}, \tag{16}$$

where λ is the wavelength. Finally, the steering vector can be written as

$$\mathbf{a}(\theta_i) = [1 \quad e^{-jkd\sin\theta_i} \quad e^{-jk2d\sin\theta_i} \quad \dots \quad e^{-jk(N-1)d\sin\theta_i}]^T \tag{17}$$

[22].

The weight vector, $\mathbf{w}$, is a function of the steering vector(s) and is further discussed in Section 2.5. The steering vector depends on the incident angle, θ, as in (17). Therefore, the mean output power, $P(\mathbf{w})$, in (9) can be written as

$$P(\theta) = \mathbf{w}^H(\theta)\mathbf{R}\mathbf{w}^H(\theta). \tag{18}$$

Radiation pattern (RP), also beam pattern, can be given in dB as

$$RP = 20\log_{10}\frac{|P(\theta)|}{\max|P(\theta)|} \tag{19}$$

[23].

2.2.4. Assumptions

The preceding analysis assumes some simplifying assumptions. However, the analysis can be utilized in less ideal environments, such as obstructed multipath environments, with some error introduced. The medium is lossless in a sense that it does not attenuate the propagating signal further than predicted by the wave equation, i.e., the signal is attenuated only inversely proportionally to the distance squared. In addition, the propagation speed is uniform. The medium is also nondispersive , i.e., it has no frequency dependency to the wave propagation. A point source is assumed to generate the propagating signal. That implies that the size of the source is small with respect to the distance between the source and antennas receiving the signal. A source produces waves that are spherical around it, however, when the antenna array is in the far-field (large distance away) of the source, these spherical waves can be approximated with plane waves. As previously discussed, the propagation delays between array elements are compensated with phase shifts. This is known as the narrowband assumption where the bandwidth of a signal is small in comparison with the carrier frequency. Thermal noise is assumed to be uncorrelated for all the array elements, as well as between them. Each element in the array has an equal, omnidirectional response. Locations of the array elements are assumed to be known perfectly as they are needed for proper delay computations. The array elements are spaced close enough so there is no amplitude variation between the signals received due to the attenuation predicted by the wave equation. No mutual coupling exists between elements. The number of signals impinging the array is finite, i.e., all the incoming signals can be decomposed into a discrete number of plane waves. [12, 14, 24, 25]

2.3. Implementation issues

2.3.1. Array geometry

Phased arrays can be formed with varying geometries. In general, they can be classified based on the number of dimensions they extend to: linear (one-dimensional), planar (two-dimensional), with geometries such as circular, rectangular and hexagonal, for example, and volumetric (three-dimensional). The elements can be spaced regularly or irregularly (randomly). Regular spacing is further subdivided into uniform and nonuniform. Phased arrays are usually arranged as a ULA, uniform circular array (UCA) or planar arrays of elements with the same polarization, low gain and orientation. Uniform arrays, while being simple, have redundant information that is avoided in minimum/null redundancy arrays (MRA/NRA). In MRA/NRA, the objective is to maximize the spatial resolution and number of spacings for the given number of elements. As an example, let us assume a four-element linear array (Figure 9 a)) is placed on the x-axis. Its elements are located at coordinates 0, 1, 2 and 3. There are three different spacings (Figure 9 b)), where spacing denotes the relative distance between elements. A spacing with distance 1 is between elements in locations 0 and 1, in locations 1 and 2, and in locations 2 and 3. The second spacing, with distance 2, exists between elements in locations 0 and 2 and in locations 1 and 3. Finally, the spacing with distance 3 exists between elements in locations 0 and 3. For each spacing, a single occurrence is enough and additional ones introduce redundancy, as is with spacings of distance 1 and 2. An array with equal length can be implemented as a NRA with three elements (Figure 9 c)) by placing them in coordinates 0, 1 and 3. In this configuration, there are 3 different spacings with distances (Figure 9 d)): 1 (between locations 0 and 1), 2 (between locations 1 and 3) and 3 (between locations 0 and 3). Each spacing exists only once and there is no redundancy. The downside of MRAs/NRAs is, that their spacings are difficult to compute, when the number of elements is high. Conversely, when the number of elements is low, the sidelobe levels are high. [3, 12, 13, 26, 27]

2.3.2. Pattern multiplication

The total radiation pattern of an antenna array is the product of the element pattern and the array factor (AF). This is known as a pattern multiplication. The element pattern is dependent on the physical dimensions and EM characteristics of the radiating element. AF depends on the amplitude, phase and position of each element in the array. Arrays can be designed without knowledge of the used antennas as a result of pattern multiplication. Pattern multiplication can also be used to determine the AF of a complicated array. A rectangular array, for example, can be considered as a linear array consisting of linear arrays. [3, 5, 9]

2.4. Performance impacting factors

A measure of the beamforming performance is a radiation pattern that depicts the gain of an adaptive array as a function of angle. In this section, the beamforming perfor-

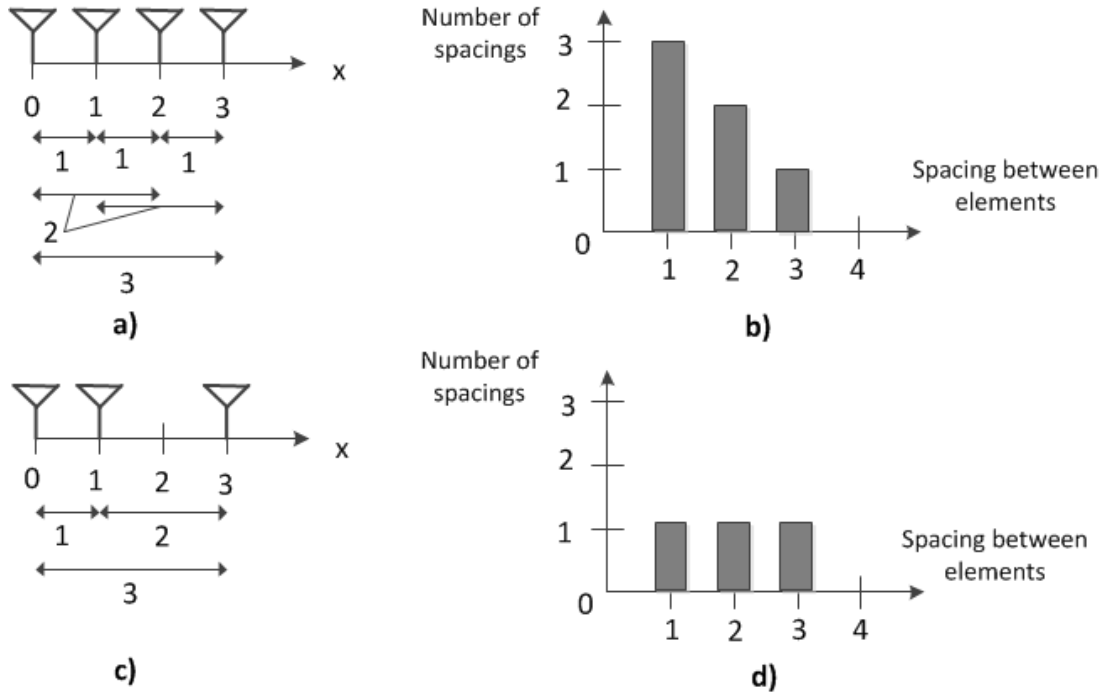

Figure 9. Uniform linear array vs. null redundancy array. (a) ULA of length 4. (b) Spatial sensitivity of the ULA. (c) NRA of length 4. (d) Spatial sensitivity of the NRA.

mance is illustrated as an array factor and the contribution of element pattern is not considered. The gain is dependent on the aperture of the array, through the number of elements and their spacings, beam's scan angle and the illumination. The performance is also measured as a beamwidth of the main beam where most of the energy is focused. Two common beamwidths are null-to-null beamwidth (NNBW) and 3 dB, also half power, beamwidth [5]. These are illustrated in Figure 10. In the following sections, each of these factors will be discussed separately for equispaced arrays.

2.4.1. Number of elements

The AF of an adaptive array can be controlled with the number of elements. Generally, the more elements it has, the better the performance. Figures 11 and 12 show the AFs for the arrays with 4, 8, 16 and 32 elements.

By increasing the number of elements, the AF has more sidelobes but their levels are lower. This improves directionality and interference is cancelled more effectively. The number of nulls is increased and they are deeper. The beams are narrower and the gain of the array is higher because of spatial diversity. The number of elements possible is constrained by a cost and physical limitations, e.g., if the array were to be mounted on an aircraft, there would an upper limit to its size. [5, 11, 12, 28]

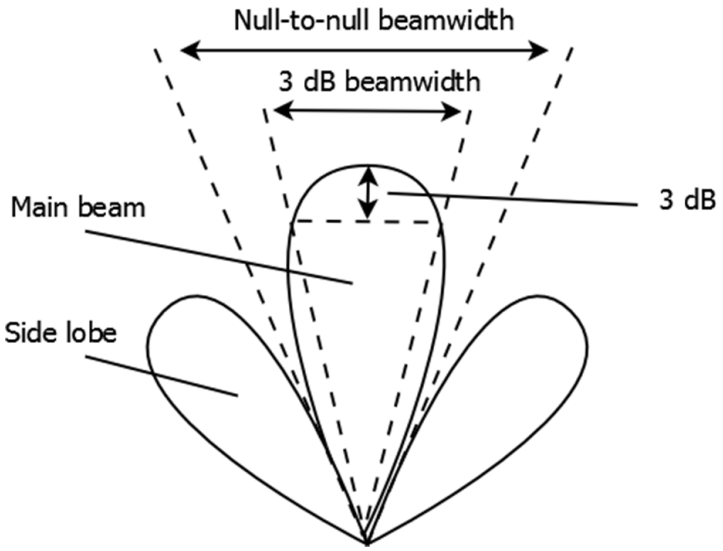

Figure 10. Null-to-null beamwidth and 3-dB beamwidth in a radiation pattern.

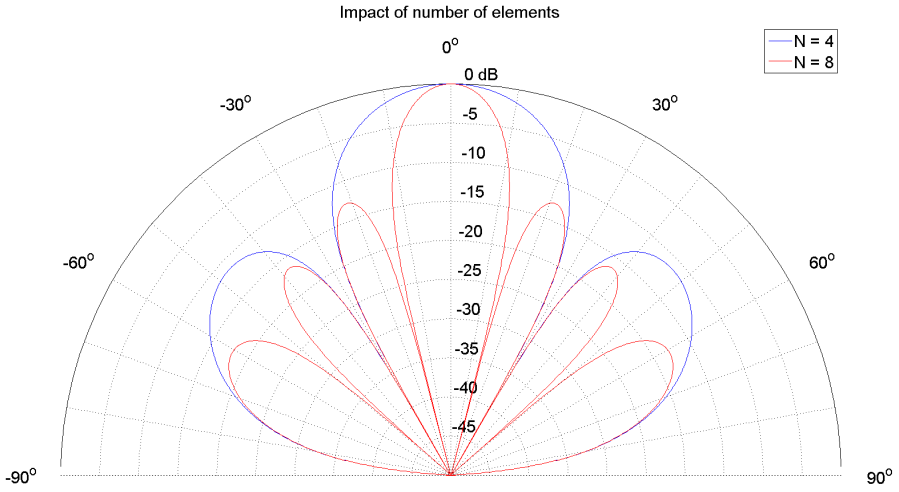

Figure 11. The array factors for 4 and 8 element arrays. Elements are spaced 0.5λ apart.

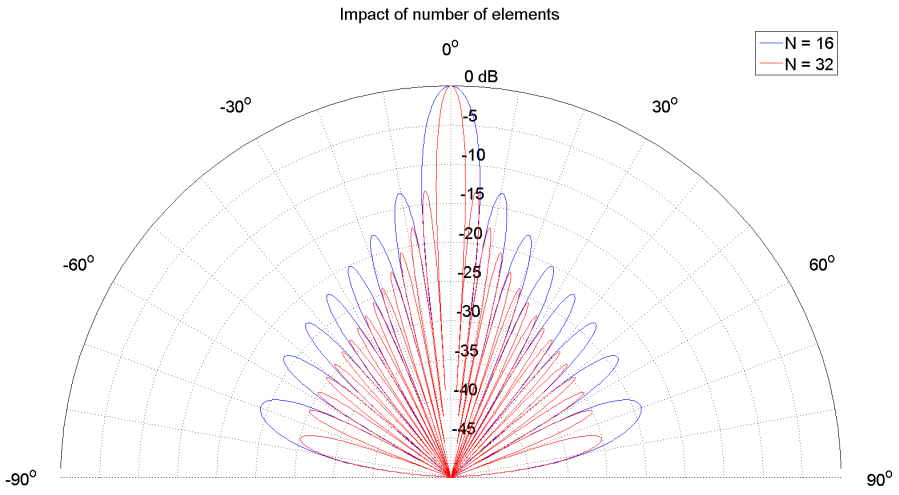

Figure 12. The array factors for 16 and 32 element arrays. Elements are spaced 0.5λ apart.

2.4.2. Element spacing

Element spacing, along with the number of elements, determines the aperture for the array. As discussed in the previous section, a larger aperture is desirable. As the spacing is increased, sidelobes, with equal gain to the main beam, appear. These are called grating lobes and their locations are periodic relative to the inverse of element spacing. In reception, the grating lobes cause directional ambiguity because the signals may come from the direction of the main beam or the grating lobe and result in the same response. In transmission, the transmitted power is wasted towards grating lobes because the receiver is on the direction of the main beam. In addition, the power transmitted towards grating lobes causes a high interference to the other users. Therefore, grating lobes are usually avoided, although they can be beneficial in some cases such as transmit diversity. [5, 9, 11, 13, 28]

The grating lobes can be prevented by reducing the element spacing. However, as the elements are closer to each other, their mutual coupling increases. In order to keep the aperture the same, to retain its properties, the number of elements needs to be increased to compensate for reduced element spacing. More elements lead to a higher cost. Hence, there is a tradeoff for choosing the element spacing. Figures 13 and 14 demonstrate the effect of the element spacing and the existence of the grating lobes. The arrays share the same aperture of 4λ but differ in the element spacing. Shorter spacings are compensated with more elements to match the aperture requirements. [9]

The existence of grating lobes is explained as a spatial aliasing that is similar to a temporal aliasing. In an analog-to-digital converter (ADC), the continuous-time signal is sampled to convert it into a discrete-time signal. Temporal aliasing occurs when the signal is sampled at a lower rate than the Nyquist sampling rate, so that two signals with different frequencies could yield the same discrete-time signal. In phased arrays, the antennas sample the impinging signals spatially. If the antennas are spaced too

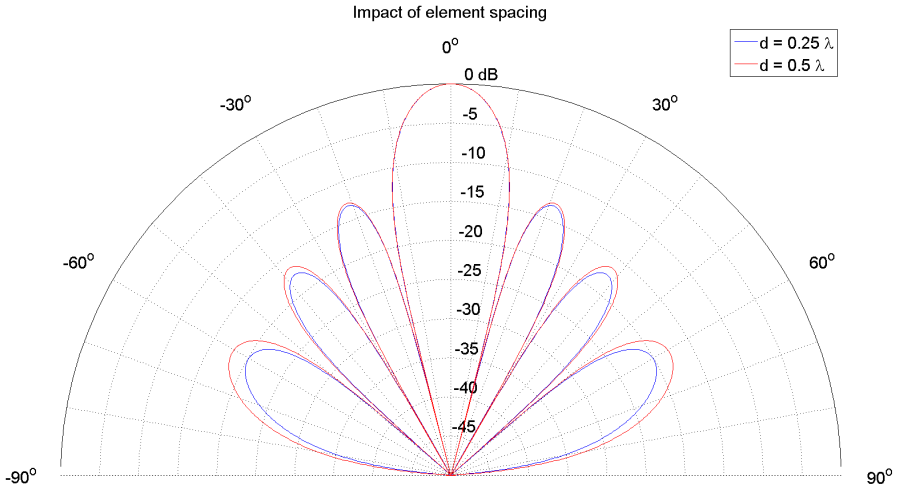

Figure 13. The array factors for arrays with element spacing of 0.25 λ and 0.5 λ. The aperture is 4λ for both arrays. No grating lobes present.

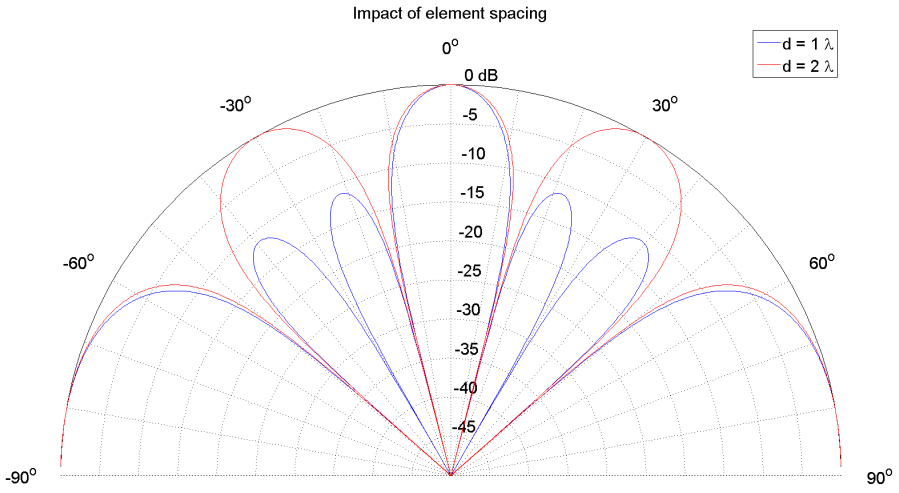

Figure 14. The array factors for arrays with element spacing of λ and 2λ. The aperture is 4λ for both arrays. Grating lobes are present in both cases: two for λ spacing and four for 2λ spacing.

far apart, the signals will not be sampled densely enough. The sources at different directions will have the same steering vector and this ambiguity in the DOAs of the sources is known as the spatial aliasing. [22]

Spatial oversampling, i.e., the spacing is less than half the wavelength, does not improve the beamformer's performance in terms of resolution. Spatial undersampling, i.e., the spacing is larger than half the wavelength, causes grating lobes. Thus, the spacing is usually chosen to be half the wavelength to maximize the aperture, yet to place grating lobes at the horizon, where they cause no harm. A uniform spacing has sidelobe level limits of -13 dB and -18 dB for the first and second sidelobes, respectively. The more the antenna array has elements, the lower the sidelobe levels are. To reduce the sidelobe levels, a non-uniform spacing can be used but with a tradeoff of increasing beamwidth. [13, 14]

As the element spacing is measured relative to the wavelength, it is dependent of the frequency. Signals with different frequencies experience the fixed spacing differently. In this thesis, narrowband systems are discussed and for wideband systems the issue needs to be addressed accordingly.

2.4.3. Scan angle

For phased arrays, the direction of the main beam, i.e., the scan angle, can be controlled with the weighting vector. As the scan angle increases the beamwidth broadens. The increased beamwidth results in a degraded performance and hence the maximum scan angle rarely exceeds $\pm 60°$. The beamwidth broadening is slower for arrays with a larger aperture. Figures 15 and 16 depict the beamwidth broadening for scan angles $0°$, $15°$, $30°$ and $45°$ with aperture size of 4λ. Figures 17 and 18 show the same but for the aperture size of 10λ. [13, 17, 29]

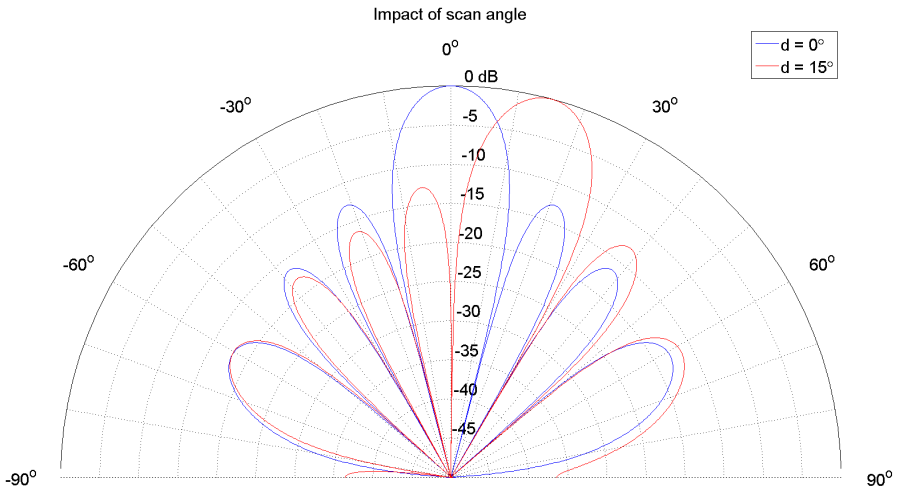

Figure 15. The array factors for an array that is scanned to angles $0°$ and $15°$. Aperture is 4λ.

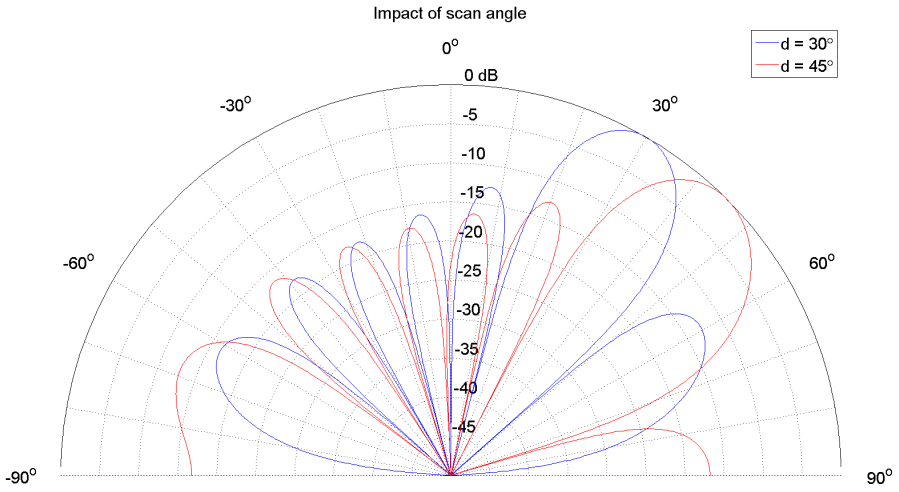

Figure 16. The array factors for an array that is scanned to angles $30°$ and $45°$. Aperture is 4λ.

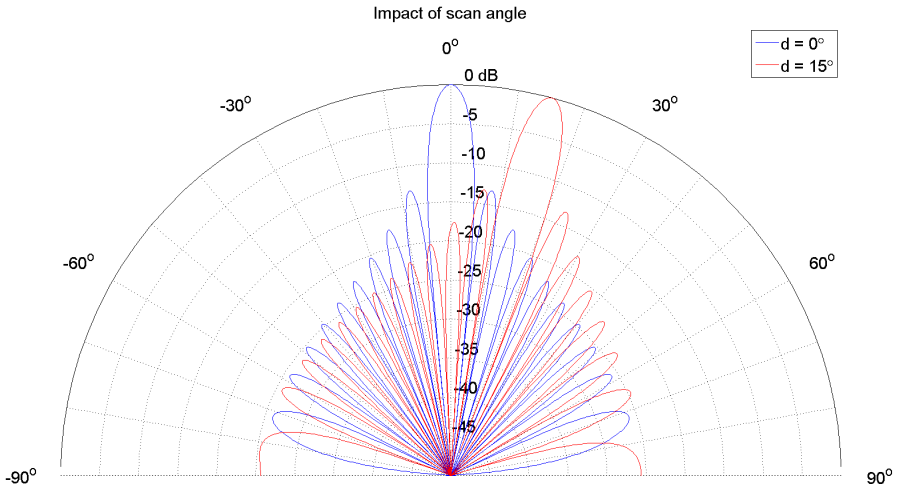

Figure 17. The array factors for an array that is scanned to angles $0°$ and $15°$. Aperture is 10λ.

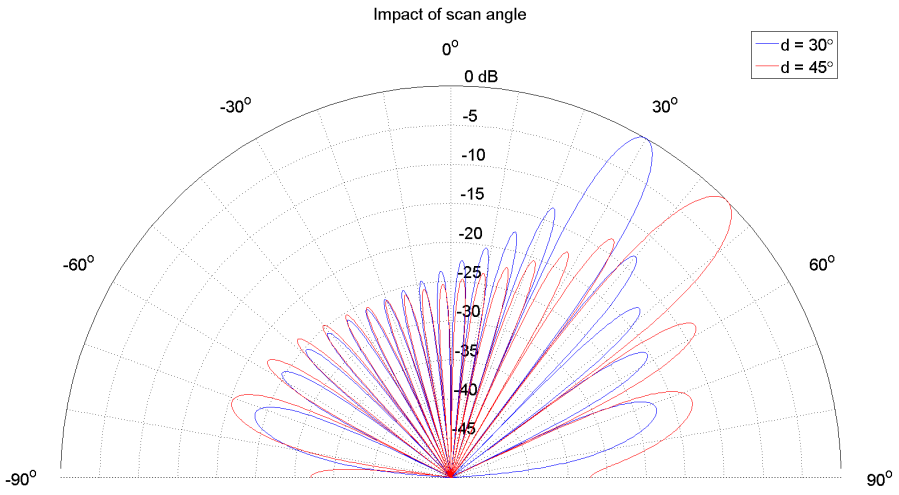

Figure 18. The array factors for an array that is scanned to angles $30°$ and $45°$. Aperture is 10λ.

2.4.4. Amplitude illumination

The amplitude illumination, the input to the antenna element, is usually constant. The sidelobe that is closest to the main beam has a level of around -13 dB (Figures 19 and 20, constant illumination). The sidelobe levels can be reduced by using an amplitude taper. Tapering is accomplished by controlling the amplitude illumination. The illumination for the element is reduced while moving away from the center of the array. Figures 19 and 20 illustrate the use of a taper for an array with 4 and 16 elements, respectively. [9, 13, 29]

Tapering produces constant sidelobe levels, where the level can be specified [11]. Lowering the sidelobe levels broadens the main beam. Beam broadening is proportional to the number of elements in the array. The less elements in the array, the larger the beam broadening is. For this reason, tapering is not usually used when the number of elements in the array is low, e.g., less than 16. The gain of the main beam no longer remains at 0 dB, but is reduced. The gain reduction is visible in RP, but not in AF. [14].

2.5. Techniques

The beamforming techniques differ in how they compute the weights and how they are applied. Computation of the weights is either non-adaptive or adaptive. Non-adaptive techniques are independent of the input data and hence suboptimal. Adaptive techniques use the a priori statistics of the data and change, or adapt, in response to the data received to derive the optimal weights. [5, 14]

Adaptive techniques use a criterion function that will optimize the spatial response of the beamformer for a maximum communication channel quality. The criterion is selected to enhance the desired signal and to minimize the contribution of interfering signals. Some commonly used criteria include minimum mean square error (MMSE),

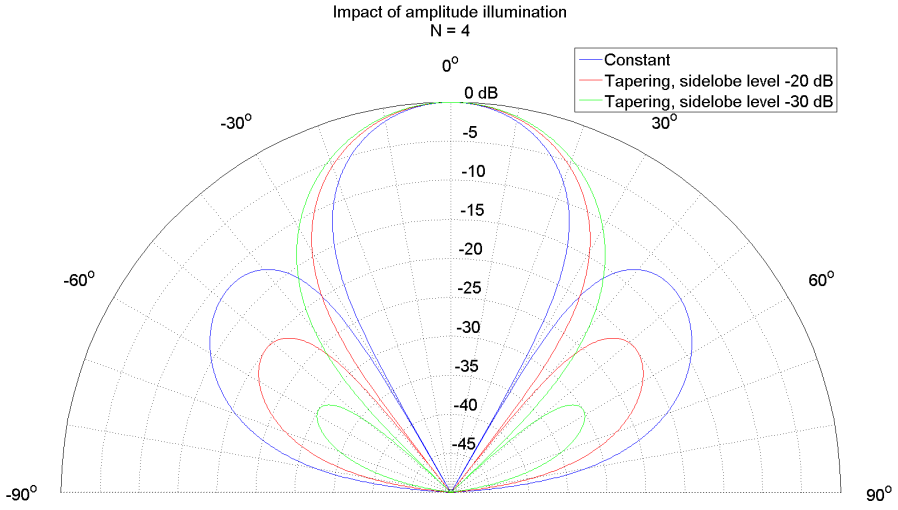

Figure 19. The array factors for an array with 4 elements. Amplitude illumination is varied between constant, -20 dB taper and -30 dB taper. Dolph-Chebyshev taper is used.

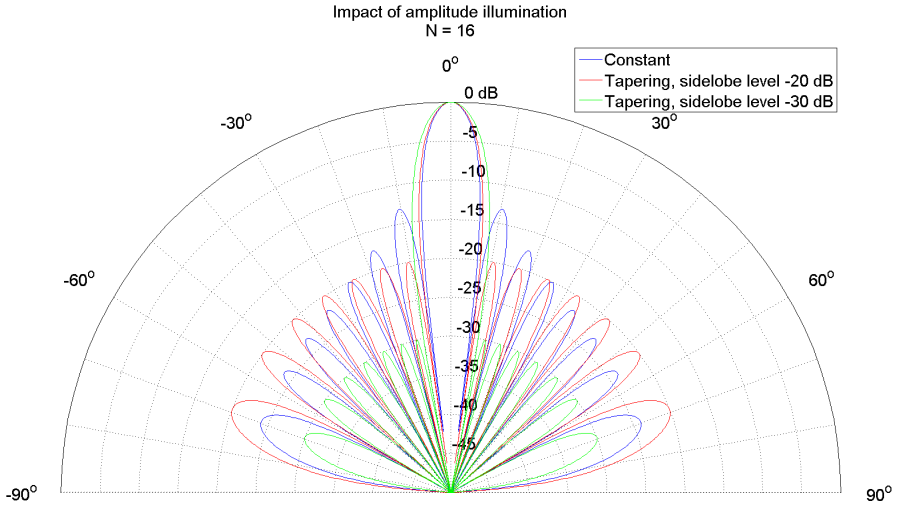

Figure 20. The array factors for an array with 16 elements. Amplitude illumination is varied between constant, -20 dB taper and -30 dB taper. Dolph-Chebyshev taper is used.

maximum SIR and minimum variance. As adaptive techniques rely on the statistics of the data, they can be classified as statistically optimal, adaptive and partially adaptive. The statistically optimal chooses the weights based on the statistics of the data. The statistics of the data are not usually known and they need to be estimated. An adaptive technique can use two methods for estimation. First is the block adaptation where statistics are estimated from a temporal block of array data and used to derive the optimal weights. Secondly, a continuous adaptation can be used, where the weights are constantly adjusted as new data arrives. The resulting weight vector sequence converges to the optimal vector. A partially adaptive uses a subset of degrees of freedom that yields a minimal loss in performance. The amount of computation is decreased and the adaptation is faster. [8, 15]

Beamforming can be implemented in two ways depending on how the weights are applied. In element-space beamforming, the weights are applied directly to the outputs of the antenna elements. For the beam-space beamformer, the outputs of antenna elements are fed into a multiple-beam beamformer to yield the orthogonal beams. Each output of the beamformer is weighted, i.e., the beams themselves. Only non-adaptive element-space beamforming techniques will be further discussed because only they are implemented. [20]

2.5.1. Conventional

The conventional beamforming is the simplest beamformer. It is also known as the classical beamformer, the delay-and-sum beamformer, the beam steering and the Bartlett's method. Steering of the beam is achieved by applying amplitudes and phases that compensate the propagation differences between the array elements and determine the look direction. Ideally, in an ULA the weights have equal magnitude and are given by

$$\mathbf{w}_C = \frac{1}{N}\mathbf{a}(\theta_0), \tag{20}$$

where N is the number of elements, $\mathbf{a}(\theta_0)$ is the steering vector and θ_0 is the incident angle of the desired signal. [5, 30]

It is assumed that only one signal source exists, with power p_s. It is located at the look direction θ_0. The signal induced on the mth element due to this source alone is

$$x_{ms}(t) = s_i(t)e^{j\omega_0(t-\tau_m(\theta_0)}. \tag{21}$$

Using vector notation and equation (14), it can be written that the signal induced on all the elements due to this source alone is

$$\mathbf{x}_s(t) = s_i(t)e^{j\omega_0 t}\mathbf{a}(\theta_0). \tag{22}$$

The beamformer output with the weight vector $\mathbf{w}_C$ is

$$y(t) = \mathbf{w}_C^H\mathbf{x}_s(t) = s_i(t)e^{j\omega_0 t}, \tag{23}$$

resulting in the mean output power to be

$$P(\omega_C) = E\{y(t) \quad y^*(t)\} = p_s, \tag{24}$$

which is equal to the source power. [23]

The conventional beamformer maximizes the signal-to-noise ratio (SNR) under special circumstances: the noise is uncorrelated and no directional interference is present. With uncorrelated noise, the noise correlation matrix is

$$\mathbf{R}_N = \sigma_n^2 \mathbf{I} \tag{25}$$

and the beamformer output noise power is

$$\mathbf{P}_N = \mathbf{w}_C^H \mathbf{R}_N \mathbf{w}_C = \frac{\sigma_n^2}{N}. \tag{26}$$

Noise power at the beamformer output is N times less than at a single element. Hence, the uncorrelated noise is reduced by N times and the beamformer output SNR is

$$SNR_{out} = p_s \frac{N}{\sigma_n^2}. \tag{27}$$

Since the input SNR is

$$SNR_{in} = \frac{p_s}{\sigma_n^2}, \tag{28}$$

the array has a gain of N. Thus, the gain of the array is directly proportional to the number of elements N, and improvements in gain, and in SNR, can be achieved with larger arrays. While conventional beamformer yields maximum output SNR with no directional interference, it will not be effective if such an interference is present. The response of the beamformer towards an interference source in a direction of θ_1 is

$$\mathbf{w}_C^H \mathbf{a}(\theta_1) = \frac{1}{N} \mathbf{a}^H(\theta_0) \mathbf{a}(\theta_1), \tag{29}$$

where $a(\theta_0)$ denotes the steering vector of a desired source and $a(\theta_1)$ that of an interferer. [23]

The main beam's beamwidth determines the resolution of the array, sources that are located closer than the beamwidth will not be resolved [27].

2.5.2. Null-steering

As in the conventional beamformer, the maximum gain is directed towards the desired signal. Additionally, minimum gains (nulls) are placed towards interfering signals to suppress them. An array with N elements is capable of producing $N-1$ nulls and therefore $N-1$ interfering sources can be eliminated. However, the DOAs of the desired signal and the interfering sources must be known. [5, 23, 30]

Null-steering beamforming can be formulated as

$$\mathbf{w}_{NS}^H \mathbf{A} = \mathbf{w}_{NS}^H [\mathbf{a}(\theta_0) \quad \mathbf{a}(\theta_1) \quad \dots \quad \mathbf{a}(\theta_{N-1})] = [1 \quad 0 \quad \cdots \quad 0], \tag{30}$$

where $\mathbf{w}_{NS}^H$ is the weighting vector, $\mathbf{A}$ is the steering matrix, $\mathbf{a}(\theta_0)$ is the steering vector for the desired signal and $\mathbf{a}(\theta_i)$ is the steering vector for the interfering signal i, where $i = 1, 2, \dots, N-1$. The desired signal is given a unity response and the interfering

signals have a zero response. The solution is straightforward if $\mathbf{A}$ is non-singular, i.e., $\mathbf{A}$ is a square matrix and all the steering vectors $a(\theta_i)$, $i = 1, 2, \ldots, N-1$, are linearly independent. Under these conditions, it results that the weighting vector is

$$\mathbf{w}_{NS}^H = [1 \quad 0 \quad \cdots \quad 0]\mathbf{A}^{-1}, \tag{31}$$

where $[\cdot]^{-1}$ denotes the matrix inversion. [5, 23]

If the number of required nulls is less than $N-1$ ($\mathbf{A}$ is not a square matrix), $\mathbf{A}$ is singular. Then, a solution can be found using a pseudo inverse, i.e.,

$$\mathbf{w}_{NS}^H = [1 \quad 0 \quad \cdots \quad 0]\mathbf{A}^{+}, \tag{32}$$

where $\mathbf{A}^+$ denotes the pseudo inverse of $\mathbf{A}$ defined as

$$\mathbf{A}^+ = \mathbf{A}^H(\mathbf{A}\mathbf{A}^H)^{-1}. \text{ [23]} \tag{33}$$

Although the interfering signals are eliminated, or at least reduced, the null-steering beamformer does not minimize the uncorrelated noise. The uncorrelated noise can be minimized by choosing weights that minimize the mean output power in addition to the aforementioned constraints. [23]

In the Figures 21 through 24, the conventional and null-steering beamformers are compared for the source directions of $0°$ and $15°$, and interference directions of $-20°$ and $-40°$. The emphasis on these two techniques is different in terms of receiving the source signal. In conventional beamforming, the main beam, with maximum gain, is steered towards the target. It does not consider interfering sources. On the other hand, the null-steering beamformer focuses on suppressing the interfering sources. While it does also steer the main beam, its performance might be sacrificed if a null is located too close to the source direction.

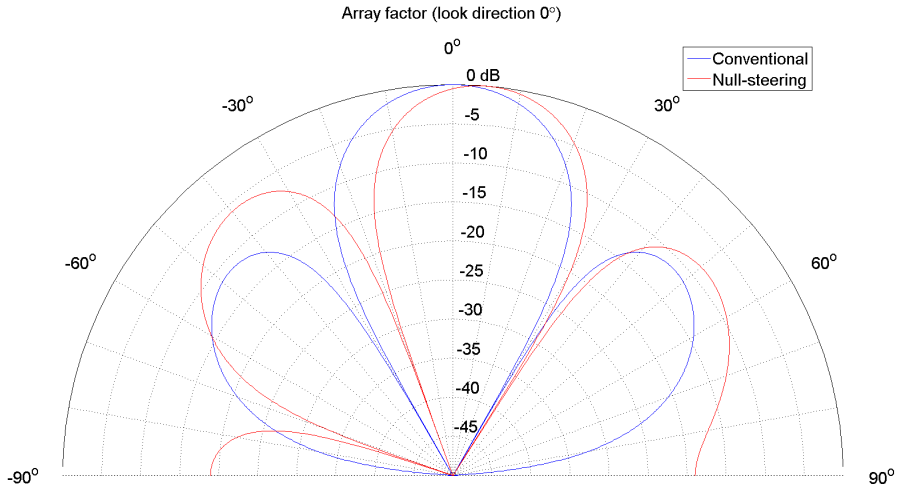

Figure 21. Conventional vs. null-steering beamforming. Source direction is $0°$ and interference direction is $-20°$.

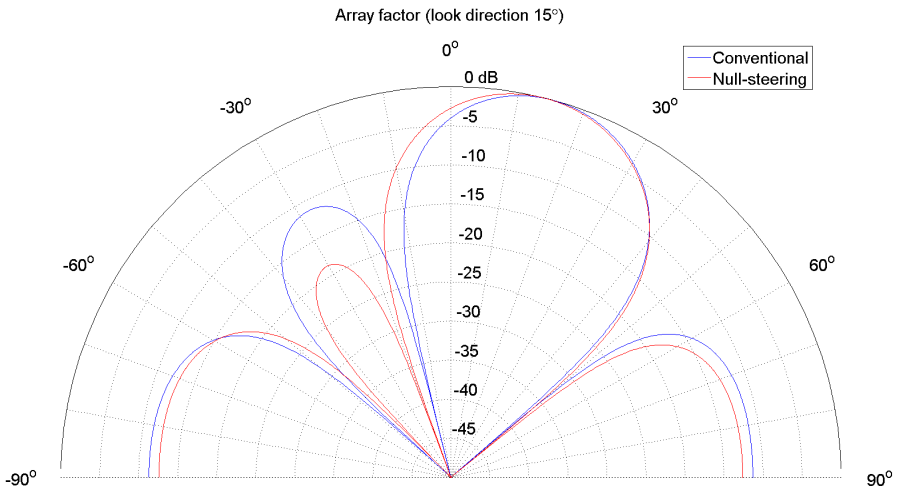

Figure 22. Conventional vs. null-steering beamforming. Source direction is $15°$ and interference direction is $-20°$.

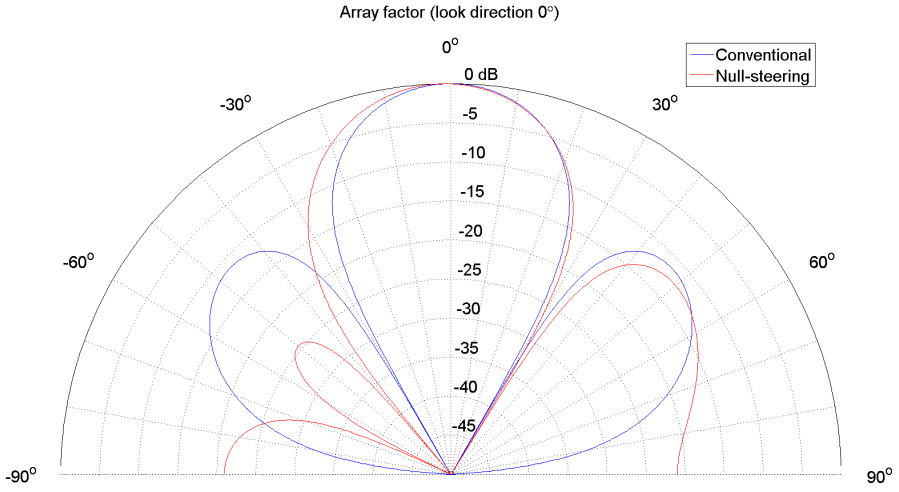

Figure 23. Conventional vs. null-steering beamforming. Source direction is $0°$ and interference direction is $-40°$.

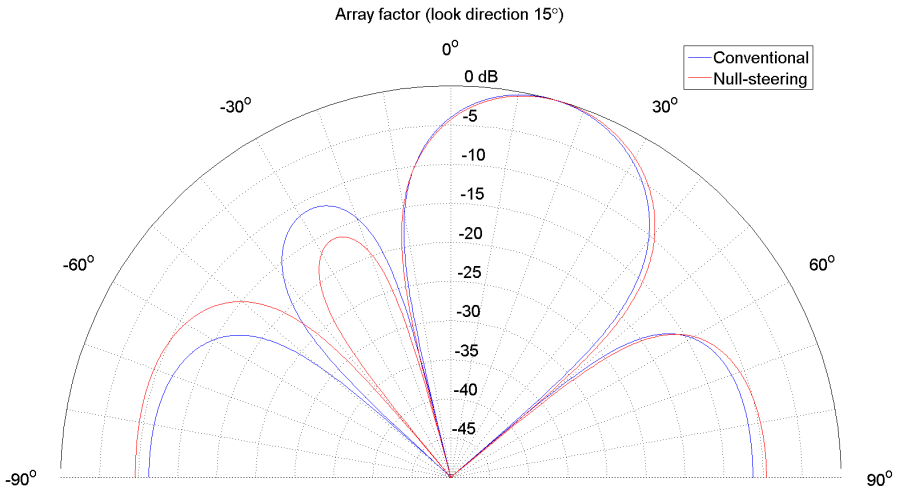

Figure 24. Conventional vs. null-steering beamforming. Source direction is 15° and interference direction is -40°.

3. WIRELESS OPEN-ACCESS RESEARCH PLATFORM

The WARP board is a wireless network research platform developed at the Rice University. It has been built around Xilinx's Virtex-II Pro FPGA. The WARP offers a platform which allows the user to modify both hardware and software. The Rice University provides a reference design for the WARP that enables researches to focus on a specific area instead of requiring them to design a complete solution. This facilitates a fast prototyping of new wireless networks. Since WARP's launch in 2005, it has gained increasing interest among researches worldwide. It has resulted in more than 75 publications [31] and is in use in more than 100 research groups in 24 countries. In 2012, the WARP users released 38 new papers and WARP papers were cited 84 times. [32]

3.1. FPGA board

A version 1 WARP FPGA board was used in this thesis and is shown in Figure 25 [33]. The core of the board is the aforementioned Xilinx Virtex-II Pro XC2VP70 FPGA. The FPGA has 5.9 Mb RAM and logic slices can be used for extra 1034 kb of additional memory. There are two banks of 18 Mb pipelined ZBT SRAM on the FPGA board. The FPGA is surrounded by four identical daughtercard slots. Below the FPGA is a slot for the clock board. [34]

The FPGA board includes several I/O devices: five push buttons, 4-position DIP-switch, four LEDs and two 7-segment displays. 10/100 Mbps Ethernet is located at the upper right corner. Other I/O include RS-232 UART and 16-bits of unbuffered 3.3V I/O connected directly to the FPGA I/O pins. The Virtex-II Pro FPGA has 8 multi-gigabit transceivers (MGT). Each MGT is a full-duplex transceiver supporting data rates up to 3.125 Gbps. The MGTs are located at the top of FPGA board. [34]

3.2. FPGA

Virtex-II family's XC2VP70FF1517-6C is a high-performance platform FPGA. Its resources include [35]:

- 33k logic slices
- 328 18x18 bit multiplier blocks
- 328 Block RAMs
- 2 PowerPC cores

The FPGA can be configured with the on-board USB configuration circuit, external JTAG cable and SystemAce CompactFlash (CF) chip. The SystemAce chip is a versatile configuration option as up to eight configurations can be stored on the CF card. The configuration is loaded automatically on power-up or via the manual reset button. The configuration is selected with a DIP switch. [34]

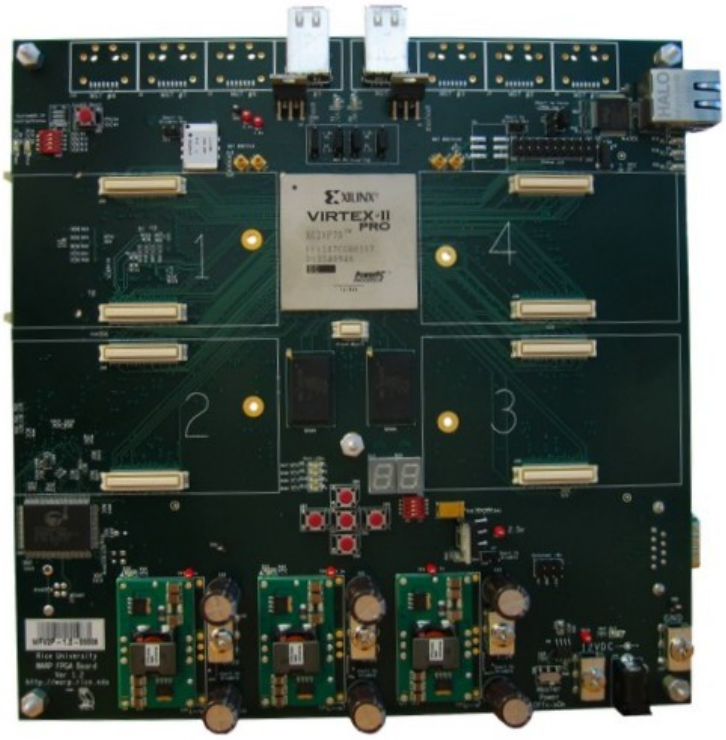

Figure 25. WARP FPGA board.

3.3. Radio board

Four available daughtercard slots on the WARP FPGA board can be equipped with radio boards. The radio board (Figure 26 [36]) provides the WARP its radio communication capabilities. The radio board's RF section consists of Maxim's MAX2829 dual-band transceiver, power amplifier and two antenna ports. Figure 27 illustrates the architecture of the radio board [36]. The key features of the transceiver are: [34]

- Dual-band (2400-2500 MHz, 4900-5875 MHz)
- Up to 40 MHz bandwidth
- Analog I/Q Tx and Rx interfaces
- 60 dB received signal strength indicator (RSSI) range
- 30 dB Tx power control range
- 93 dB Rx gain control range
- MIMO capable

The radio board can be controlled with two custom peripherals: a radio controller and a radio bridge. The radio controller uses SPI logic to manipulate radio and digital-to-analog converter (DAC) chip registers. In addition, it tracks the control pins of both

Figure 26. Radio board.

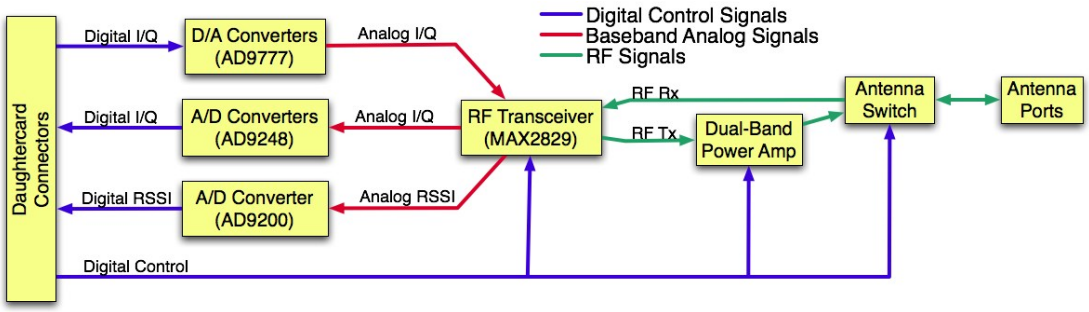

Figure 27. Radio board architecture.

chips. The radio controller does not directly connect to the radio board, but utilizes the radio bridge as a proxy. The separation of control logic and connections to different peripherals enables the use of a single controller to control all the radio boards. [34]

The WARP FGPA board can accommodate varying number of radio boards and as such the radio boards have been designed to be modular. Each of the radio boards is equipped with its own phase-locked loop (PLL). The PLLs are not phase synchronized to each other, which is a disadvantage in phased array designs. For beamforming, the phase differences need to be taken into account.

3.4. WARPLab

WARPLab is a framework combining WARP with MATLAB. WARP nodes are controlled directly from the MATLAB workspace. Signals to be transmitted are generated in MATLAB and passed to WARP nodes via Ethernet links. Transmission is in real-

time over-the-air (OTA) with WARP nodes. Novel physical layer (PHY) implementations can be implemented and tested quickly with the MATLAB M-code. [37]

WARP nodes and a PC running MATLAB are connected to a switch via Ethernet links. Up to 16 WARP nodes can be connected to a single PC. Figure 28 depicts the WARPLab architecture [37].

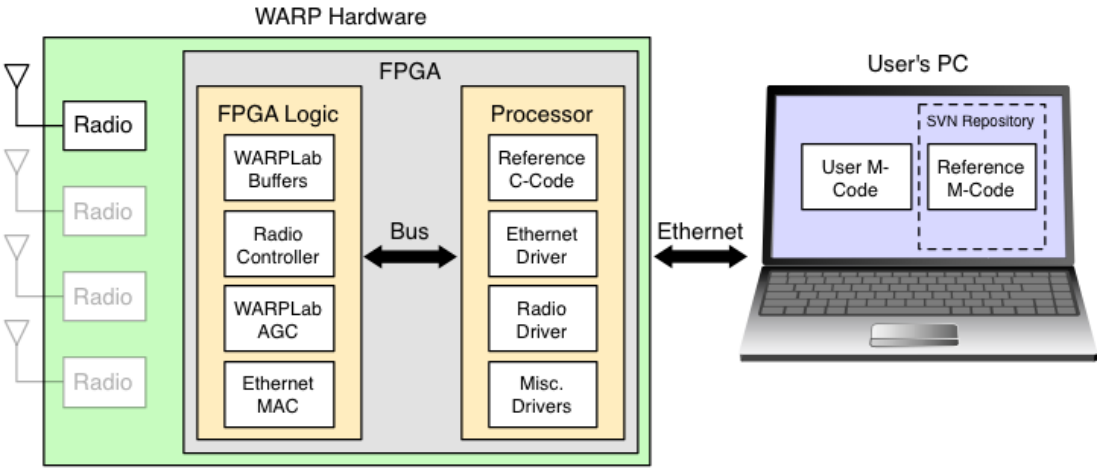

Figure 28. WARPLab architecture.

Ethernet links are used to transfer the data between a PC and WARP nodes. The data can be signal samples or control information. [37]

Transmission samples are generated in MATLAB and transferred to transmitting WARP nodes' buffers. A trigger is sent to both transmitting and receiving WARP nodes. The trigger commences transmission and reception simultaneously. The transmission and capture of samples happen in real-time OTA. Captured samples are stored into buffers in receiving WARP nodes. The samples are transferred to a PC, where they are processed offline in MATLAB. [37]

A reference design for both the WARP nodes and MATLAB is provided by the Rice University. The reference design for the FPGA provides functions such as Tx and Rx buffers, radio controller, automatic gain control (AGC) and Ethernet MAC as FPGA logic. The reference M-code enables the control and interaction with the WARP nodes on a PC. Both of these reference designs can be modified and extended as needed. WARPLab does not enable real-time sample processing since the samples need to be transferred between WARP nodes and a PC. The reference design for FPGA can be modified if real-time functionality is required. Hence, WARPLab can be used for prototyping a design before it is implemented on the FPGA. [37]

4. CALIBRATION

So far, the discussion about beamforming has expected ideal conditions. In practice, this is rarely, if ever, the case. The adaptive array has to be calibrated to minimize the effects of nonidealities.

Antenna element hardware and cables can introduce amplitude and phase mismatch [38–41]. The position of the antenna element or the signal DOA might be uncertain [38–40]. A close proximity of antenna elements causes mutual coupling, i.e., electromagnetic interaction and increases with smaller inter-element spacing [38, 39, 41, 42]. The metal of the tower, the antenna array is mounted on, can affect the radiation pattern and is known as the tower effect [43].

The calibration can be performed using different techniques. Some techniques isolate the error sources and compensate the effects one at a time while others handle multiple error sources simultaneously. A common method is to place the transmitter at a known location relative to the antenna array. The response of the antenna array can be compared against the expected response of an ideal array. The difference can be used as an estimate for the distortion experienced in the array. Finally, it can be compensated to yield a close to ideal array. In practice, a multipath propagation can introduce unknown distortion unless eliminated, for example, using an anechoic chamber for measurements. Additionally, the transmitter needs to reside in the far-field of the array for correct beamforming operation. Another common method is to inject a signal to all the array channels with an equal phase. The measured array outputs can be used to estimate the amplitude and phase distortions. Other methods include using known environmental reflectors, multiple scattering sources and blind techniques. [38, 39]

The calibration performed in this thesis comprises the calibration of the PLLs found in each radio board on the WARP and the calibration of the antenna array that is known as the array manifold measurement.

4.1. Phase-locked loop calibration

Implementing beamforming on the WARP board required additional calibration due to its modular design. Each of the antenna array antennas was connected to its own radio board with its own PLL. Each of the radio boards was driven by the same clock and they were frequency synchronized but not phase synchronized. As beamforming is based on controlling the amplitude and phase between different antennas, it is vital that any phase offsets among radio boards are compensated.

The PLLs lock with a random phase offset whenever WARP is powered on or the channel is changed. The phase offset remains constant until the PLL locks again. A phase synchronization was achieved by choosing one of the radio boards as a reference and synchronizing others to it. Figure 29 demonstrates random phase offsets in PLLs and synchronization to reference.

Each of the PLLs has a random phase offset, α_i, that is independent of the others. The PLL of radio board 1 was selected as the reference to whom others are synchronized to.

The PLLs were phase synchronized by pairing up radio boards and transmitting a reference signal between them. The radio boards were connected to each other via

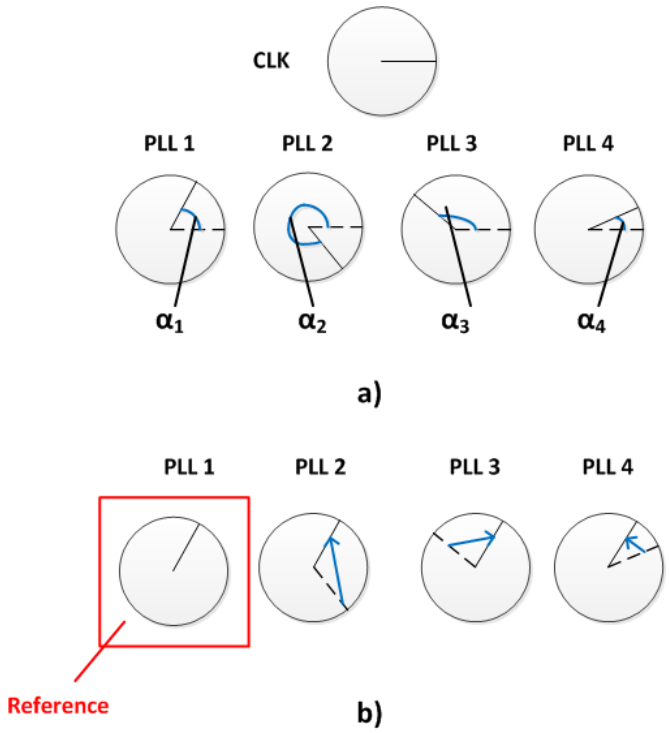

Figure 29. (a) Random phase offsets in the PLLs with respect to clock. (b) Reference selection and synchronization.

a coaxial cable and an attenuator to remove the effect of the radio channel. Table 1 depicts the phase offset measurement setups used in the phase synchronization.

The measurements are numbered as #X, where X denotes the measurement number. For every measurement, there is a transmitter and receiver radio, denoted by numbers in Tx and Rx columns, respectively. Phase offsets are measured for radios 2, 3 and 4 with respect to reference radio 1. Phase offset is an addition of two measurements, where a measurement indicated with $+$ contributes as is and a measurement indicated with $-$ contributes as complemented.

Figure 30 shows the phase offset measurement #1 setup.

Table 1. Phase offset measurement setups

	Radio mode		**Phase offset**		
Measurement	*Tx*	*Rx*	*2 vs 1*	*3 vs 1*	*4 vs 1*
#1	1	3	-		-
#2	2	3	+		
#3	4	3			+
#4	3	4		+	
#5	1	4		-	

In order to phase synchronize radio board 1 (reference) and radio board 2, two measurements (#1 and #2) were required. In measurement #1, the radio board 1 transmitted

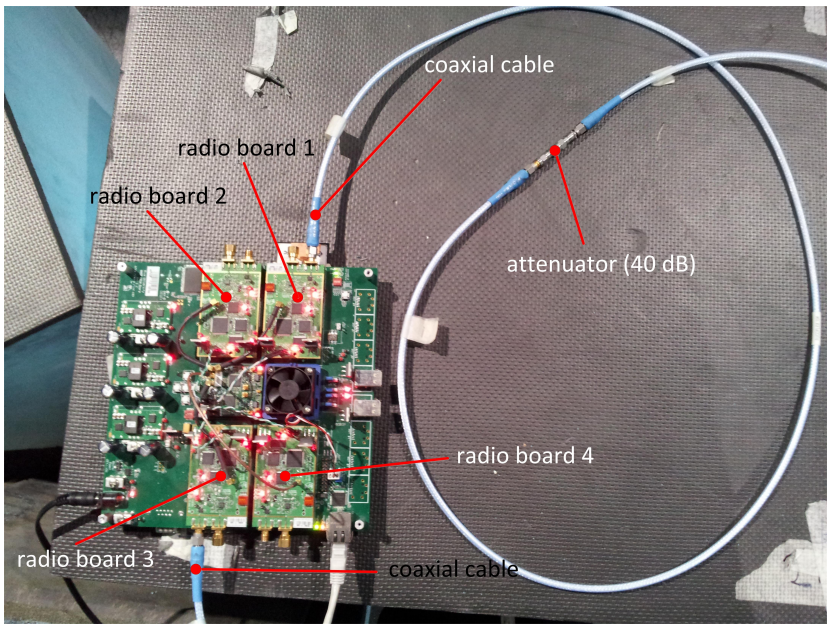

Figure 30. PLL phase offset measurement #1 setup.

a reference signal to the radio board 3. The received signal's phase at the radio board 3 was compared against the known phase of the reference signal to determine the phase shift from radio board 1 to 3. In measurement #2, the same operation was performed except now the radio board 2 was the transmitter. The phase offsets from measurements #2 and #1 were added together according to table 1, i.e., the phase offset from measurement #2 as is and the phase offset from measurement #1 as complemented. Finally, the aforementioned addition yielded the phase offset for the PLL 2 with respect to the reference PLL 1. The phase offsets for the PLLs 3 and 4 with respect to the reference PLL 1 could be resolved with the same procedure utilizing measurements as shown in table 1.

Figure 31 details the pairwise measurements explained above. In Figure 31 a) and b), the phase offset between two radio boards is measured. The factors affecting the measured phase offset are separated. On the transmitter side, the phase changes due to the transmitter PLL in the upconversion stage, denoted as α_i and α_j in Figure 31 a) and b), respectively. On the receiver side, the phase changes due to a reverse operation in the downconversion stage and propagation delay. The phase offset in the downconversion stage is denoted as α_k in both Figure 31 a) and b). Its sign is a complement to that in upconversion stage because of reverse operation. The PLLs advance their phases continuously and the receiver side PLL experiences a delay while the signal propagates. As the signal arrives at the receiver PLL, after propagation, its phase is no longer the same as it was during a reference point in the transmitter PLL. The change in phase is perceived erroneously as an additional phase offset denoted as δ.

Figure 32 illustrates the effect of propagation delay. The unit circles on the left side represent the phases of PLLs while the signal is at the transmitter upconversion stage. The right side unit circles represent the phases of PLLs while the signal is at the receiver downconversion stage. Both of the PLLs have their phases advanced by δ. The receiver side angle rotates in the opposite direction as the transmitter side angle

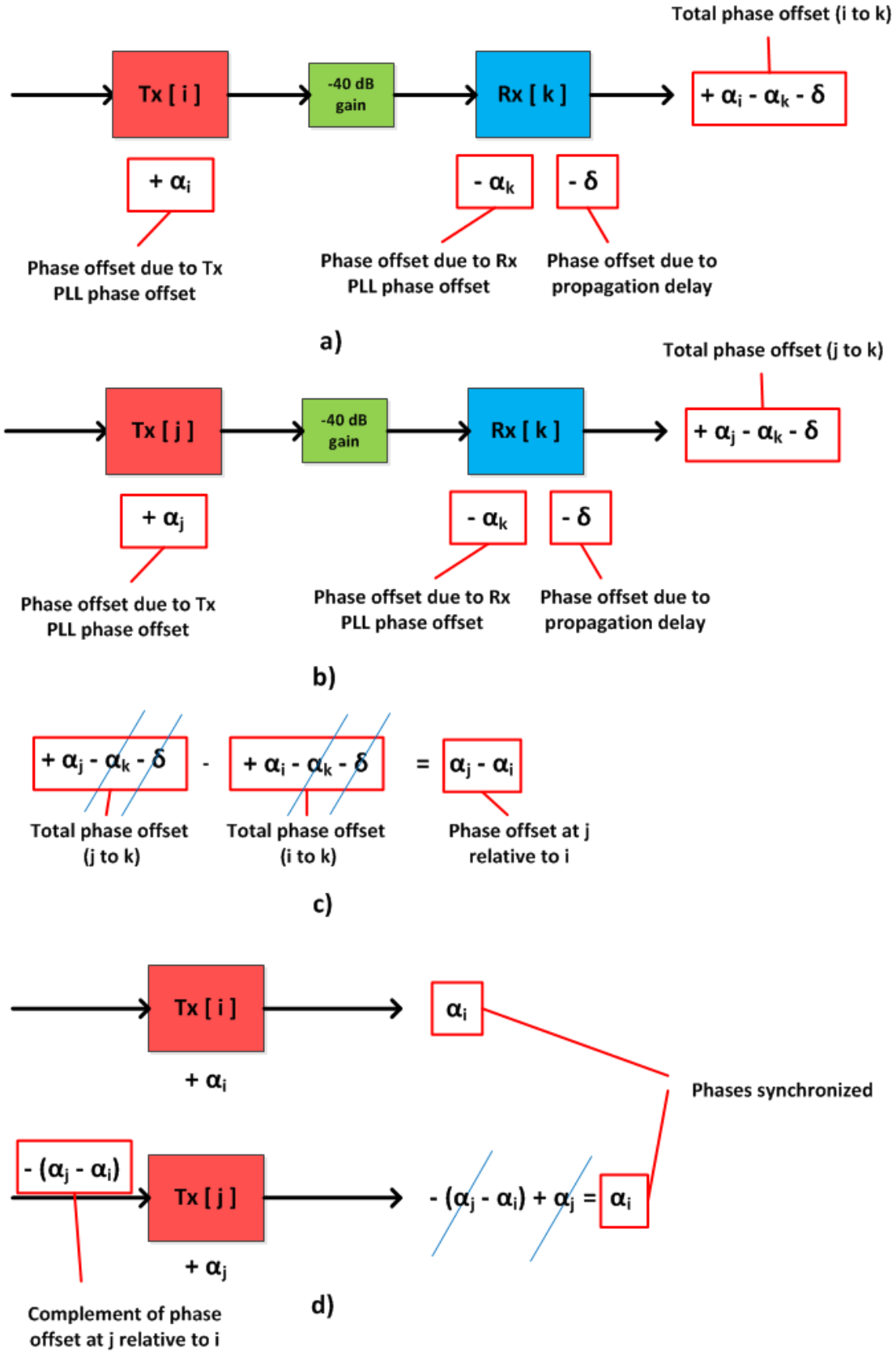

Figure 31. (a) Phase offset measurement between radio boards i (Tx) and k (Rx). (b) Phase offset measurement between radio boards j (Tx) and k (Rx). (c) Phase offset at radio board j relative to radio board i. (d) Phase compensation to match radio board j to reference radio board i.

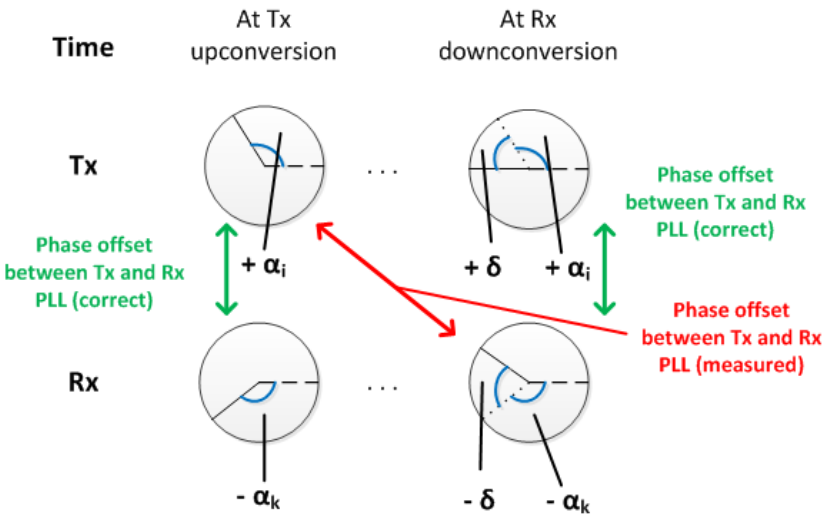

Figure 32. The effect of propagation delay in phase offset measurement.

since the downconversion performs a reverse operation compared with the upconversion. The correct phase offset between the transmitter and receiver PLLs would be determined by comparing the phases at the same time instant. However, the signal is not available for analysis until the end of path. Thus, the measurement yields, as the phase offset, the combined effect of all three factors. To eliminate the contribution of unknown propagation delay to the phase offset, two measurements are performed. The measurements differ only in transmitting radio board. Hence, the phase offsets differ only with phase offset between different transmitters as is shown in Figure 31 c). After the phase offset between two radio boards is known, their phases can be synchronized by applying the complement of the phase offset (Figure 31 d)).

4.2. Array manifold measurement

The antenna array was calibrated by measuring its response for each DOA. The set of steering vectors, for each DOA, is known as the array manifold. The measurement was performed in an anechoic chamber to avoid errors due to multipath components and interference. The purpose of the array manifold measurement was not to make the antenna array ideal by compensating the nonidealities. Instead, the acquired steering vectors included the effects of nonidealities and were used to derive the beamforming weights. The beamforming weights took into account the effects of nonidealities.

Figure 33 represents the measurement configuration. On the transmitter side, a single omnidirectional antenna transmitted a reference signal. The transmitter antenna was positioned perpendicularly towards the antenna array's center. The antenna array, consisting of four identical omnidirectional antennas, spaced half the wavelength apart, operated as the receiving side and was rotated $180°$ around its center. As the array was rotated counterclockwise, the DOA of the transmitter signal changed and the array's response was measured for each DOA. The array manifold was measured for DOAs in range of $[-90°, 90°]$ with $5°$ intervals as an average of 100 samples. Since the main

beam's beamwidth is large for a four-element ULA, a 5° interval was chosen to result in adequate precision. In Figures 34 and 35, the array manifold measurement in an anechoic chamber is represented from the point of view of the transmitter antenna and the antenna array, respectively.

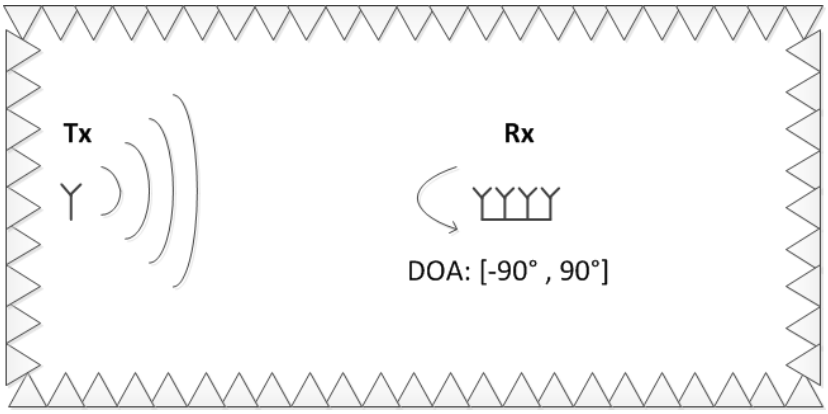

Figure 33. Array manifold measurement in an anechoic chamber. The antenna array (Rx) is at the starting position for the measurement. The DOA of the signal from transmitter is now -90°. The antenna array is rotated 180° counterclockwise.

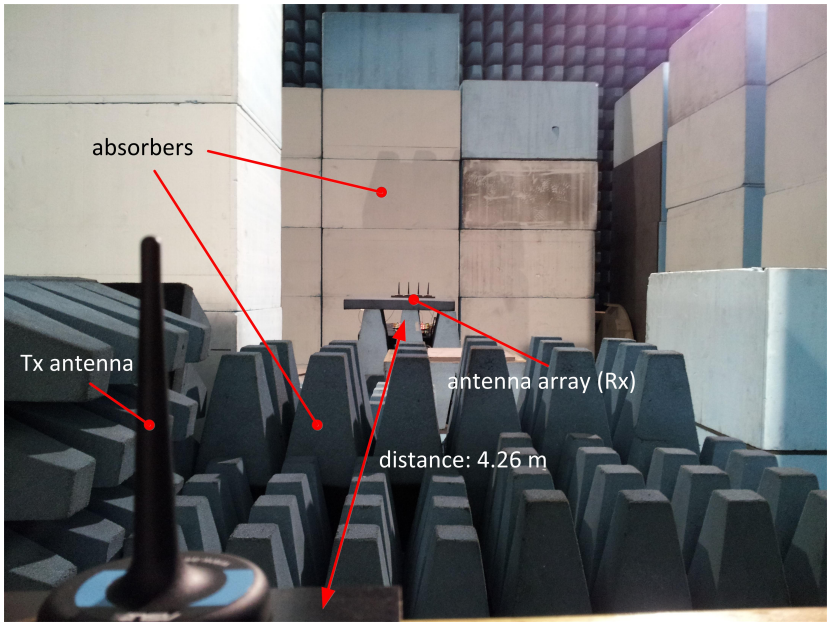

Figure 34. Array manifold measurement in an anechoic chamber from the point of view of the transmitter antenna.

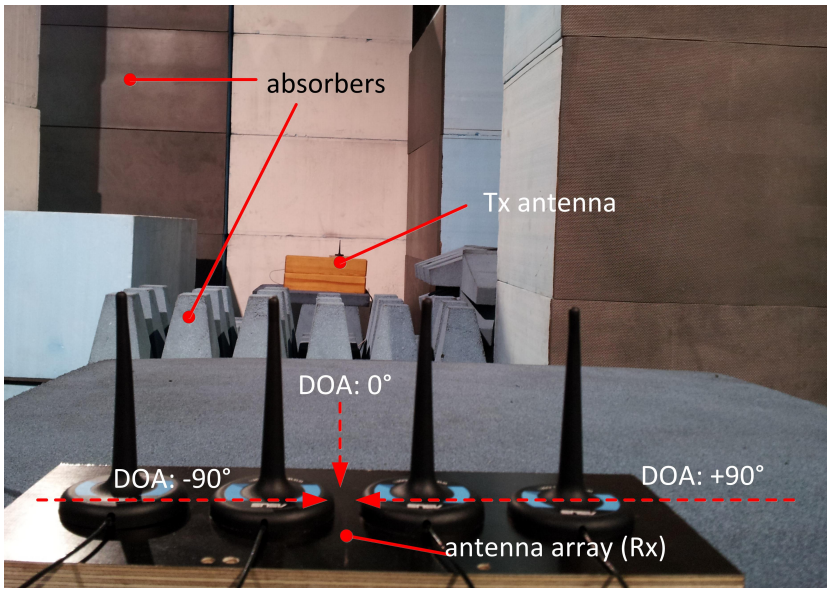

Figure 35. Array manifold measurement in an anechoic chamber from the point of view of the antenna array. The used antenna array can be seen in this figure.

5. MEASUREMENTS

The WARPLab implementation of beamforming algorithms was evaluated by measuring the transmitted and received beamform of the antenna array for the DOA of $0°$. The measured radiation patterns were compared against the ideal ones. The measurements were performed in an anechoic chamber to eliminate the effects of multipath propagation and interference.

Section 5.1 explains the setup used in the measurements. The receive and transmit beamforming results, for both conventional and null-steering beamforming algorithms, are presented in Sections 5.2 and 5.3, respectively.

5.1. Measurement setup

The setup is equivalent to the array manifold measurement described in Section 4.2 except now both the single omnidirectional antenna and the antenna array can operate as a receiver and transmitter. In receive beamforming, the antenna array operates as the receiver and the single antenna as the transmitter. For transmit beamforming, the operations are reversed. Figure 36 shows the measurement setup in an anechoic chamber.

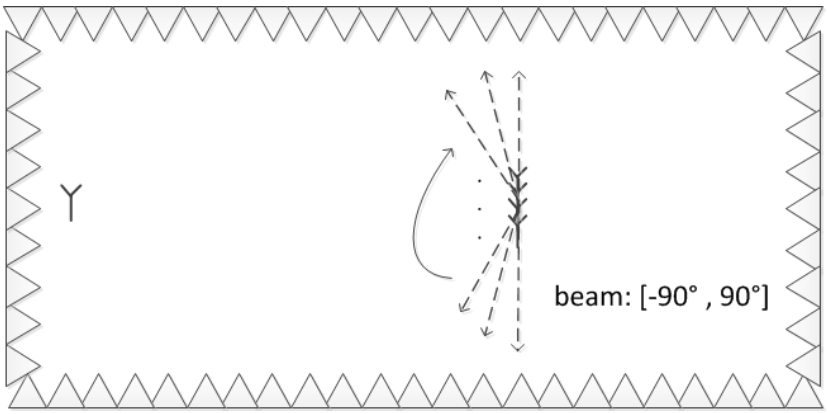

Figure 36. Beamform measurement setup in an anechoic chamber.

The radiation pattern was formed by a series of power measurements for DOAs in range of $[-90°, 90°]$ with $5°$ intervals. There are two methods for performing these measurements. In the first method, both the single antenna and the antenna array remain in place. The antenna array is positioned orthogonally towards the single antenna so that DOA of $0°$ is the direction of the single antenna. The beam is rotated by selecting a different steering vector. The radiation pattern can be measured rapidly and the measurements result in the actual beamform for the DOA of $0°$. This method was used for the conventional beamforming.

The radiation pattern for different DOAs was simulated in MATLAB. In the conventional beamforming, the radiation pattern remained intact considering power measurements at DOA of $0°$ while the beam was rotated. However, in the null-steering, the radiation pattern changed considerably and the aforementioned measurements would

yield an erroneous radiation pattern. The second method is to rotate the antenna array while the beam remains stationary towards the broadside. Now the radiation pattern change at the DOA of $0°$ is avoided but the downside is that the measurements take longer due to a physical rotation of the beam. The second method was used for the null-steering.

5.2. Receive beamforming

Four different beamforming measurements were performed. The conventional beamform was measured once for a beam with DOA of $0°$. The null-steering beamforming measurements included three scenarios. The first scenario had two nulls at DOAs of $-50°$ and $50°$. The second scenario had one null at DOA of $45°$. The third scenario had three nulls at DOAs of $-60°$, $-30°$ and $30°$. In all three null-steering scenarios, the main beam had a DOA of $0°$.

All the beamform figures include three different curves. The ideal curve (green) represents a theoretical curve computed in MATLAB under perfect conditions. The practical curve (blue) denotes a possible beamform for the measured array manifold. The beamforming weights are derived from the measured array manifold and a steering vector for DOA of $0°$ is used as the signal. The curve is dependent of the measuring conditions for the array manifold. The measured curve (red) is the actual measured beamform and it is dependent of the measuring conditions for both the array manifold and the signal.

The receive beamform for the conventional beamforming is given in Figure 37. The receive beamforms for the null-steering beamforming scenarios are illustrated in Figures 38 through 40.

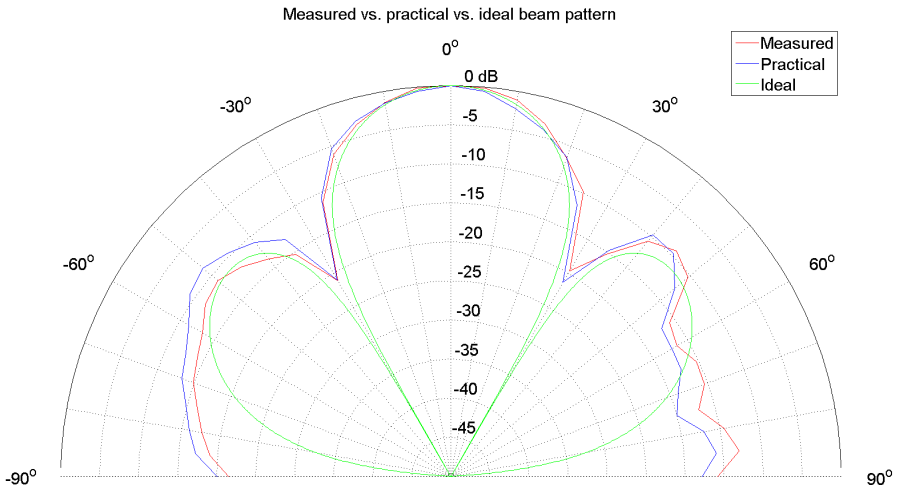

Figure 37. Receive beamform for conventional beamforming.

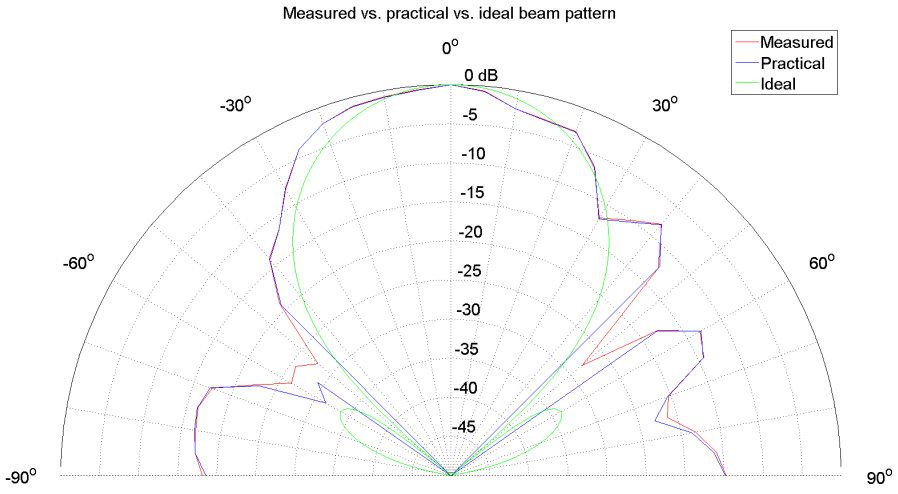

Figure 38. Receive beamform for null-steering beamforming. Two nulls are at DOAs of $-50°$ and $50°$.

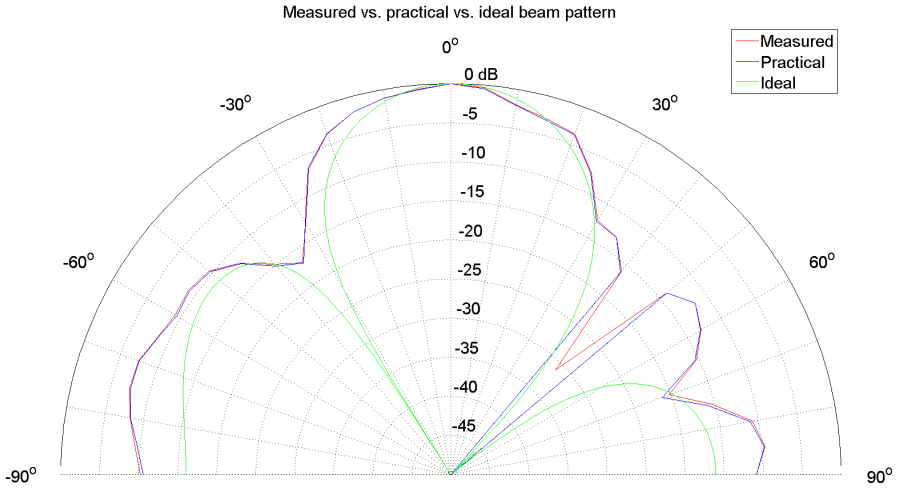

Figure 39. Receive beamform for conventional beamforming. One null is at DOA of $45°$.

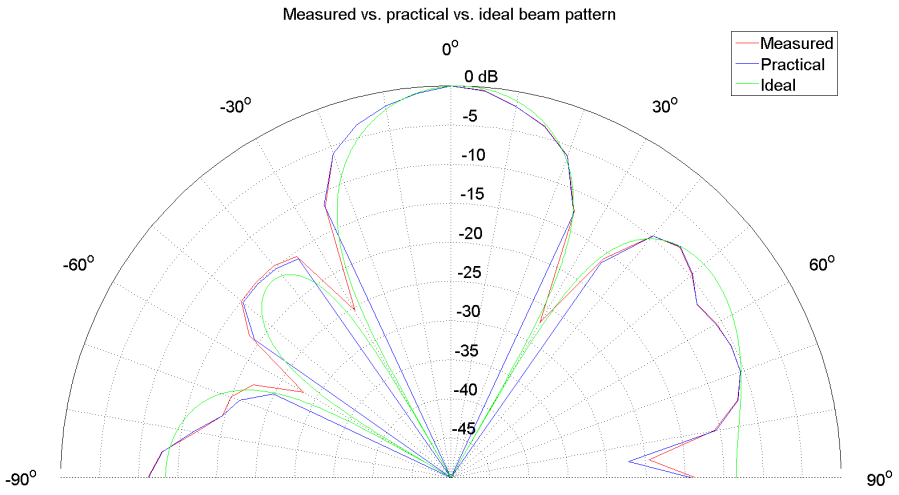

Figure 40. Receive beamform for conventional beamforming. Three nulls are at DOAs of $-60°$, $-30°$ and $30°$.

5.3. Transmit beamforming

Transmit beamforming was unsuccessful and the results do not meet the expectations for neither the conventional nor the null-steering beamforming algorithms. Below are the observed beamforms for the conventional beamforming and the null-steering beamforming scenarios one and two in Figures 41 through 43. The third scenario was not measured as it was irrelevant based on the results of earlier scenarios. The ideal and practical curves seen in the figures are the same as in the receive beamforming figures due to reciprocity. The reasons for unsatisfactory transmit beamform performance is a topic for future work.

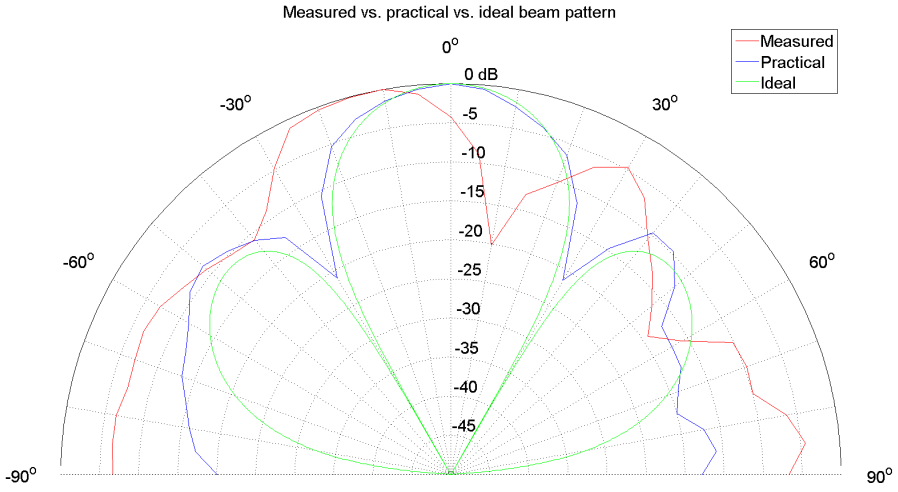

Figure 41. Transmit beamform for conventional beamforming.

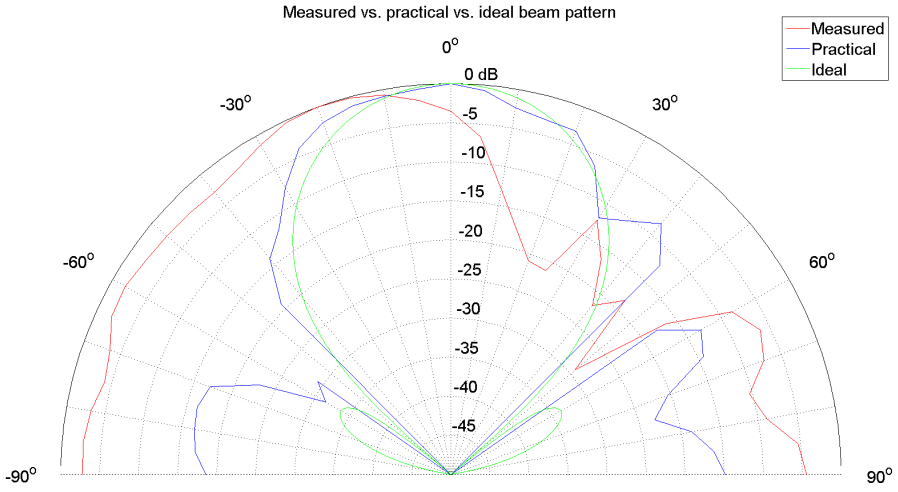

Figure 42. Transmit beamform for null-steering beamforming. Two nulls are at DOAs of $-50°$ and $50°$.

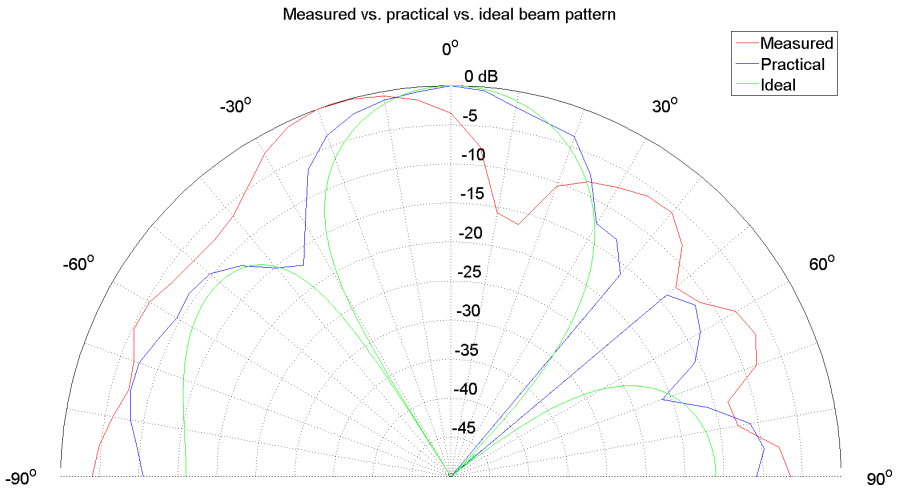

Figure 43. Transmit beamform for conventional beamforming. One null is at DOA of $45°$.

6. DISCUSSION

The conventional and null-steering beamforming algorithms were implemented with the WARP board. A four-element ULA, consisting of omnidirectional antennas, acted as the antenna array. The operation of beamforming algorithms was evaluated in anechoic chamber measurements.

Even though the beamforming algorithms implemented were of the simplest kind, the antenna array required a rigorous calibration. Such a calibration could not be performed in normal operating conditions because of interference and multipath propagation. Therefore, a controlled environment, such as an anechoic chamber, was required.

The antenna array was calibrated by measuring its array manifold. It was used to derive the weights for both receive and transmit beamforming. Hence, their performance was limited by the accuracy of the antenna array calibration. Based on the measured array manifold, practical beamform curves were derived for the conventional and null-steering beamforming. Compared with the ideal beamforms, practical beamforms yielded a good main beam performance although for null-steering there were some deviations. The null levels were about -21 dB for the conventional beamforming and below -50 dB for the null-steering. The sidelobe levels were slightly high and wide for the conventional beamforming. In null-steering, the sidelobe levels were somewhat or considerably higher and wider depending on the scenario. The measured receive beamforming curves followed practical ones quite closely, except for the null-steering, the nulls were much higher, at around -28 dB. The measured transmit beamforming curves did not agree with the practical ones.

The primary tasks were the implementation of receive and transmit beamforming. The receive beamforming operated as expected but the transmit beamforming did not and requires additional exploration. The radio board had separate paths for transmission and reception. During the array manifold measurement, the signal traveled on the reception path and equivalently on the receive beamforming. Both of the paths have the same operations, only reversed. The array manifold measurement was only affected by the reception path and the measurement was used to derive weights for both the receive and transmission beamforming. Now, if the signal paths differed in their effects on the signal, other than what can be explained by the reverse operation, it might be that transmit beamforming would require its own kind of array manifold measurement to operate correctly.

Another major task, discovered during the thesis, was the PLL phase synchronization issue. Unlike in traditional beamforming systems, the WARP board had a separate PLL for each of the antennas due to its modular design. The PLLs were not phase synchronized to each other, making the beamforming impossible unless the phase offsets were estimated and compensated.

After the array manifold and beamforms were measured, the WARP was rebooted to force the PLLs to re-lock. The PLL phase offsets were random and new after the power cycle. The weights, based on the array manifold measured last time, were used again for the receive beamforming. The receive beamform was not correct and it was necessary to measure the array manifold again for this power cycle. The weights derived from the newly measured array manifold yielded the proper receive beamform suggesting that the PLL phase offset compensation was not successful. The implementation

would be unpractical if the array manifold would have to be measured again, every time the WARP is powered on, since the measurement requires an anechoic chamber.

The array manifold was measured again without the PLL phase offset compensation. In this case there would be phase offsets present during the array manifold measurement. The receive beamform was measured again using the weights derived from the new array manifold measurement. The receive beamform was correct even though phase offsets were present supporting the idea that the array manifold would also factor in the effects of the phase offsets among the PLLs. Therefore, no phase offset compensation would be necessary if the antenna array were to be calibrated every time it is powered on. The antenna array calibration could not be reused because it considers the phase offsets present during the calibration and the phase offsets are new and random after the WARP is powered on again. Alternatively, the antenna array could be calibrated once if the phase offsets remained the same, e.g., by the PLL calibration.

In its current state the antenna array is not practically viable for demonstrations since the array requires a calibration in an anechoic chamber and the WARP must stay powered on. However, the implemented beamforming algorithms demonstrate the potential of SDMA techniques for improving the capacity in future wireless communication networks. The improvement is not only limited to allowing more users to communicate simultaneously in the same area, but the interference is also reduced, enabling the use of more complex modulation schemes.

7. SUMMARY

The purpose of this thesis was to develop a reconfigurable antenna system capable of directional transmission and reception. By utilizing direction selective communications, major performance improvements are possible in cognitive radio networks. Multiple simultaneous transmissions can be active in the same area as long as they do not occupy the same space.

The challenge to meet the ever-growing requirements for capacity was the motivation behind new SDMA methods. Earlier SDMA methods included sectorization and basic smart antenna techniques using one or more fixed beams that were switched to as needed. Advanced smart antenna techniques can steer the beams instead of switching between fixed beams.

An adaptive array utilizing beamforming is one of the advanced smart antenna techniques. Its fundamentals were introduced. Other factors considered were the signal model, implementation issues and performance impacting factors. The adaptive array could be implemented in various geometries of which the ULA was chosen. The radiation pattern of a single element affects the whole radiation pattern of an adaptive array, known as pattern multiplication. The performance is dependent of the number of elements, element spacing, scan angle and amplitude illumination.

Two different beamforming techniques were presented. The conventional beamformer, also known as the delay-and-sum beamformer, steers the main beam towards the target. In the null-steering algorithm, the focus was on suppressing the interfering sources by steering nulls toward undesired targets.

The adaptive array was implemented as a four-element ULA of omnidirectional antennas. The antennas were controlled with the WARP board. The implementation utilized WARPLab, where the WARP nodes could be controlled in MATLAB over Ethernet.

The WARP's control of antennas was implemented via separate radio boards. Each of the radio boards had its own PLL so they were not phase synchronized by default. One of the PLLs was selected as a reference and the others were phase synchronized to it with pairwise measurements between multiple radio boards.

Another calibration was required to minimize the effect of nonidealities in the adaptive array. Its response for each DOA was measured in an anechoic chamber to form the array manifold.

Receive and transmit beamforms were measured in an anechoic chamber. The receive beamforms were as expected in both the conventional beamforming and null-steering algorithms. However, the transmit beamforms did not meet the requirements and need further work. The receive beamforms could not be repeated when the WARP board was rebooted unless the antenna array was recalibrated. A possible reason might be that the PLL phases were not properly calibrated and the antenna array calibration was dependent on the previous power cycle PLL phases, that were renewed at the reboot.

8. REFERENCES

[1] Cisco visual networking index forecast projects 18-fold growth in global mobile internet data traffic from 2011 to 2016 (accessed 26.9.2012). URL: http://newsroom.cisco.com/press-release-content?type=webcontent&articleId=668380.

[2] Halim M.A. (2001) Adaptive array measurements in communications. Artech House, Norwood, MA, first ed.

[3] Litva J. & Lo T.K.Y. (1996) Digital beamforming in wireless communications. Artech House, Norwood, MA, first ed.

[4] George Tsoulos M.B. & McGeehan J. (1997) Wireless personal communications for the 21st century: European technological advances in adaptive antennas. IEEE Communications Magazine 35, pp. 102–109.

[5] Zooghby A.E. (2005) Smart antenna engineering. Artech House, Norwood, MA, first ed.

[6] Active antenna systems: A step-change in base station site performance (accessed 12.10.2012). URL: http://www.nokiasiemensnetworks.com/sites/default/files/document/nokia_siemens_networks_active_antenna_system_white_paper_26_01_12_0.pdf.

[7] What is beamforming? (accessed 13.8.2012). URL: http://users.ece.utexas.edu/~bevans/courses/ee382c/lectures/12_pn/allen/Beamforming/index.html.

[8] Haynes T. (1998) A primer on digital beamforming. Spectrum Signal Processing, http://www.spectrumsignal.com.

[9] S. Drabowitch A. Papiernik H.G. & Encinas J. (1998) Modern antennas. Chapman and Hall, Boundary Row, London, first ed.

[10] Okamoto G.T. (1999) Smart antenna systems and wireless LANs. Kluwer Academic, Norwell, MA, first ed.

[11] Antenna-theory (accessed 14.8.2012). URL: http://www.antenna-theory.com/.

[12] Joseph C. Liberti J. & Rappaport T.S. (1999) Smart antennas for wireless communications: IS-95 and third generation CDMA applications. Prentice Hall, Upper Saddle River, NJ, first ed.

[13] Fourikis N. (2000) Advanced array systems, applications and RF technologies. Academic Press, London, GBR, first ed.

[14] Dimitris G. Manolakis V.K.I. & Kogon S.M. (2005) Statistical and adaptive signal processing: spectral estimation, signal modeling, adaptive filtering and array processing. Artech House, Norwood, MA, first ed.

[15] VanVeen B.D. & Buckley K.M. (1988) Beamforming: a versatile approach to spatial filtering. IEEE Acoustics, Speech and Signal Processing Magazine 5, pp. 4–24.

[16] Matlab (accessed 20.9.2012). URL: http://www.mathworks.com/.

[17] Hansen R.C. (2009) Phased array antennas. Wiley, Hoboken, NJ, second ed.

[18] Kildal P.S. (2000) Foundations of antennas: a unified approach. Studentlitteratur, Lund, first ed.

[19] Wikipedia: beamforming (accessed 6.8.2012). URL: http://en.wikipedia.org/wiki/Beamforming.

[20] Vavrda M. Digital beamforming in wireless communications. Institute of Radio Electronics, Faculty of Electrical Engineering and Communication.

[21] T. K. Sarkar M. C. Wicks M.S.P. & Bonneau R.J. (2003) Smart antennas. Wiley, Hoboken, NJ, first ed.

[22] Liu W. & Weiss S. (2010) Wideband beamforming concepts and techniques. John Wiley and Sons, Hoboken, NJ, first ed.

[23] Godara L.C. (1997) Application of antenna arrays to mobile communications, part II: beam-forming and direction-of-arrival considerations. Proceedings of the IEEE 85, pp. 1195–1245.

[24] Compton R.T. (1988) Adaptive antennas: concepts and performance. Prentice-Hall, Englewood Cliffs, NJ, first ed.

[25] Piper J.E. (2011) Beamforming narrowband and broadband signals. Naval Surface Warfare Center (NSWC).

[26] VanTrees H.L. (2002) Optimum array processing, part IV of detection, estimation and modulation theory. John Wiley and Sons, New York, NY, first ed.

[27] Krim H. & Viberg M. (1996) Two decades of array signal processing research. IEEE Signal Processing Magazine 13, pp. 67–94.

[28] The lab book pages: microphone array beamforming (accessed 15.8.2012). URL: http://www.labbookpages.co.uk/audio/beamforming.html.

[29] Mailloux R.J. (2005) Phased array antenna handbook. Artech House, Norwood, MA, second ed.

[30] Puska H. (2009) Code acquisition in direct sequence spread spectrum systems using smart antennas. Ph.D. thesis, Faculty of Technology, Department of Electrical and Information Engineering, University of Oulu.

[31] Wireless open-access research platform: papers and presentations (accessed 7.8.2012). URL: http://warp.rice.edu/trac/wiki/PapersandPresentations.

[32] Warp project (accessed 7.8.2012). URL: http://warpproject.org.

[33] Wireless open-access research platform: Fpga board (accessed 19.9.2012). URL: http://warp.rice.edu/trac/wiki/HardwareUsersGuides/FPGABoard_v1.2.

[34] Wireless open-access research platform: wiki (accessed 8.8.2012). URL: http://warp.rice.edu/trac/.

[35] Virtex-ii pro fpga: datasheet (accessed 19.9.2012). URL: http://www.xilinx.com/support/documentation/data_sheets/ds083.pdf.

[36] Wireless open-access research platform: radio board (accessed 20.9.2012). URL: http://warp.rice.edu/trac/wiki/HardwareUsersGuides/RadioBoard_v1.4.

[37] Warplab framework overview (accessed 20.9.2012). URL: http://warp.rice.edu/trac/wiki/WARPLab.

[38] Kapil R. Dandekar H.L. & Xu G. (2000) Smart antenna array calibration procedure including amplitude and phase mismatch and mutual coupling effects. Personal Wireless Communications , pp. 293–297.

[39] Richard B. Ertel Z.H. & Reed J.H. (1999) Antenna array hardware amplitude and phase compensation using baseband antenna array outputs. Vehicular Technology Conference 3, pp. 1759–1763.

[40] Yuan-Hwang Chen A.C.C. & Lee H.T. (2000) Array calibration methods for sensor position and pointing errors. Microwave and Optical Technology Letters 26, pp. 132–137.

[41] Zeyang D. & Yuming D. (2009) Fast active calibration for uniform linear array with amplitude and phase errors. Proceedings of the 2009 International Workshop on Information Security and Application , pp. 349–352.

[42] Mutual coupling in antenna arrays (accessed 15.11.2012). URL: http://www.ece.nus.edu.sg/stfpage/elehht/Teaching/EE6832/Lecture Notes/MutualCouplinginAntennaArrays.pdf.

[43] Shively labs: Uhf antenna choices (accessed 15.11.2012). URL: http://www.scribd.com/doc/8616071/Tbuhf-Antenna-Choices.